INTERNAL DYNAMICS AND BOUNDARY FORCING CHARACTERISTICS ASSOCIATED WITH INTERANNUAL VARIABILITY OF THE ASIAN SUMMER MONSOON

K.-M. Lau , K.-M. Kim[1] and S. Yang[2]

Climate and Radiation Branch

NASA/Goddard Space Flight Center

Greenbelt, MD 20771

October, 1998

(submitted to J. Climate)

Corresponding author address: Dr. K.-M. Lau, NASA/GSFC, Climate and Radiation Branch, Code 913, Greenbelt, MD 20771

[1] Universities Space Research Association, NASA/GSFC, Greenbelt, MD

[2] SAIC/General Sciences Corporation, Laurel, MD

ABSTRACT

In this paper, we present a description of the internal dynamics and boundary forcing characteristics of two major components of the Asian summer monsoon (ASM), i.e., the South Asian (SAM) and the Southeast-East Asian monsoon (SEAM). The description is based on a new monsoon-climate paradigm in which the variability of ASM is considered as the outcome of the interplay of a "fast" and an "intermediate" monsoon subsystem, under the influenced of the "slow" varying external forcings. Two sets of regional monsoon indices derived from dynamically consistent rainfall and wind data are used in this study. For SAM, the internal dynamics is represented by that of a "classical" monsoon system where the anomalous circulation is governed by Rossby-wave dynamics, i.e., generation of anomalous vorticity induced by an off-equatorial heat source is balanced by planetary vorticity advection. On the other hand, the internal dynamics of SEAM is characterized by a "hybrid" monsoon system featuring multi-cellular meridional circulation over the East Asian section, extending from the deep tropics to midlatitudes. These meridional cells link tropical heating to extratropical circulation system via the East Asian jetstream, and are responsible for the characteristic occurrences of zonally oriented anomalous rainfall patterns over East Asian and the subtropical western Pacific. In the extratropical regions, the major upper level vorticity balance is by anomalous vorticity advection and generation by the anomalous divergent circulation. A consequence of this is that compared to SAM, the SEAM is associated with stronger teleconnection patterns to regions outside the ASM.

A strong SAM is linked to basin-scale sea surface temperature (SST) fluctuation with significant signal in the equatorial eastern Pacific. During the boreal spring SST warming in the Arabian Sea and the subtropical western Pacific may lead to a strong SAM. For SEAM, interannual variability is tied to SSTA over the Sea of Japan and the South China Sea regions, while the linkage to equatorial basin-scale SSTA is weak at best. A large scale SSTA dipole with warming (cooling) in the subtropical central (eastern) Pacific foreshadows a strong SEAM

Comparative analyses with the Webster and Yang (1992) monsoon index (WY) show that WY is not significant correlated neither with the SAM or SEAM regional scale rainfall. We found that WY is more appropriate as a measure of the large scale atmospheric circulation state of the Indian/Pacific Ocean basins, in which the ASM is an integral part. As such, WY together with the regional monsoon indices developed in this paper provide a complementary description of the broad scale and regional aspects of the ASM.

A key conclusion from the present study is that interannual variabilites of major subcomponents of the ASM, i.e., SAM and SEAM, are governed not only by basin scale SSTA, but perhaps more strongly by coupled SSTA in the sub-tropical western Pacific, the South China Sea and the Arabian Sea. These represent regions where additional predictability of the ASM should be more fully exploited.

1. Introduction

It is well known that the Asian summer monsoon (ASM) is an extremely complex phenomenon which encompasses variabilities over a wide range of spatial and temporal scales. Prediction of the monsoon is one of the major challenges of climate research. Recently numerous studies have suggested that the El Nino-Southern Oscillation (ENSO) may have an influence on the year-to-year variability of the ASM (Rasmussen and Carpenter, 1982, Webster and Yang 1992, Ju and Slingo 1995, Lau and Bua 1998, and others). These studies have also shown that many extreme ASM drought and flood occurrences may not be linked to ENSO. By some estimate, more than half of the major anomalies in the ASM are not related to ENSO, suggesting that there are other factors that may contribute to the predictability (or lack thereof) of the ASM.

Heuristically, variabilities of the ASM can be classified in terms of those due to internal dynamics and those forced by boundary conditions such as sea surface temperature (SST) and land surface conditions (Shukla 1984, Palmer 1994). For seasonal-to-interannual predictions, the former constitutes the chaotic or unpredictable component, while the latter, the potentially predictable component of the ASM. The degree to which the ASM is controlled by each component determines the overall predictability of the system.

One difficulty encountered in the predictability of the ASM is that monsoon variability itself cannot be easily quantified because it is a strong function of space and time, as well as dependent on the parameters used. For long-term monsoon variability, many authors used the all-India monsoon rainfall (AIMR) as an index for the ASM (Mooley et al. 1986, Parthasarathy et al. 1992, Lau and Yang 1996 and many others). However, because the Indian subcontinent covers only a small fraction of the entire ASM region, it may not be representative of the variability of the ASM as a whole. Likewise, results from variability studies using East Asian rainfall (e.g., Shen and Lau 1994, Nitta and Hu 1996 and Weng et al. 1998) may not be applicable to other regions of the ASM. During the warm event of 1997, rainfall averaged over the entire Indian subcontinent was near normal. Yet, the monsoon over the East Asian and the southeast Asian regions were

extremely abnormal with record breaking droughts and floods in different parts of East Asia (C.-Y. Li, private communication). This is so, despite the Indian monsoon is known statistically to have a stronger ENSO influence compared to the East Asian monsoon (Ropelewski and Halpert 1988).

The aforementioned considerations beg the following questions: What do we really mean by long-term variability of the ASM? Does there exist a meaningful, quantitative measure that describes the ASM system as a whole? As its individual sub-components? Are there distinctly different dynamical characteristics for different regional components of the ASM?. How do these different regional characteristics relate to lower boundary forcings such as SST. In this paper, we will address and explore answers to these questions.

2. Preliminary considerations

In an attempt to quantify monsoon climate variability, a number of authors have used different monsoon indices to quantify different components of the ASM (Webster and Yang 1992, Goswami et al., 1998, Ailikun and Yasunari 1998). The present paper is an attempt to synthesize and to expand on some of the concepts developed in these studies. To begin, we propose a new paradigm for classification of the ASM based on characteristics of its internal dynamics, local and remote boundary forcing functions.

a. A monsoon climate paradigm

The basic concept of this paradigm is illustrated in Fig. 1, which encapsulates a monsoon-centric view of the climate system including its sub-components. This schematic presumes a basic knowledge of the ASM. For detailed description of the individual phenomena, the readers are referred to various review papers of the ASM in the literature (e.g. Krishnamurti 1985, Lau and Li 1984, Webster et al. 1998 and many others). At the center of the climate system shown in Fig. 1 is the ASM which, for completeness, includes both the summer and the winter components, hence the annual

5

cycle label. The ASM is affected by the "fast system", depicted in the lower left-hand corner of the schematic. This is the internal dynamic subsystem which includes moisture recycling and hydrologic feedback in the monsoon atmosphere. This fast system is dominated by synoptic (3-5 days), subsynoptic to cloud scales (< 1 day) and can be identified with monsoon depressions, easterly waves, convective cloud clusters, meso-scale complexes within the ASM regions. Additionally, the monsoon climate is strongly affected by surface conditions in the adjacent oceans and land masses, represented as the "intermediate" subsystem in the lower right-land corner of Fig. 1. This subsystem possesses both fast and slow (weeks to months) time scales. The key constituents in this subsystem consist of SST, wind and surface humidity which determine heat and moisture fluxes over the adjacent oceans, i.e., the Indian Ocean, the South China Sea and the western Pacific warm pool. Also pertinent to the "intermediate" system is the effects of soil moisture, vegetation and snow cover which control the heat and moisture flux over the land regions of ASM.

Connecting the fast and intermediate subsystems is "intraseasonal variability" which includes the Madden and Julian Oscillations (MJO) and other atmospheric low-frequency variability such as the biweekly oscillations, which have been linked to onset, breaks and revival of the ASM. Both the fast and intermediate subsystems are under influence of remote forcings from planetary scale phenomena such as ENSO and other long-term secular variations of the global climate system from decadal variability to global warming. These remote forcings constitute the "slow" subsystem that is external to the ASM, but yet can play an important role in altering the basic states of the monsoon atmosphere, the adjacent oceans and land surfaces. These altered states may then lead to modulations of the probability distribution of monsoon states within the "fast system". It is also plausible that the coupling of the fast and intermediate subsystems may influence the "slow system". These two-way interactions are represented by the linkages labeled "teleconnections" in Fig. 1. As an example, SST anomalies in the Indian Ocean, and the western Pacific may be coupled to ENSO either through Walker-type atmospheric circulation and/ or via oceanic throughflow near Indonesia and the Philippines. Another example is the possible linkage between the equatorial east-west SST gradient across the

6

Pacific basin and the meridional thermocline gradient through subduction processes originating in the extratropical oceans (Liu and Huang 1997, Gu and Philander 1997). These gradients define the basic oceanic state which governs long-term behavior of ENSO-monsoon interactions.

In the aforementioned paradigm, interannual predictability of the monsoon climate is determined by the strength of the linkages provided by the intermediate and the slow subsystems. The predictability of the monsoon climate evolves as the result of an inter-play between the relative influence of the fast, the intermediate and the slow components. The stronger control by the fast system, the less predictable is the ASM. The more influence by the slower subsystems, the more the ASM is predictable. In this view, the predictability of the monsoon evolves as a function of the slow varying basic statesand therefore will wax and wane over long time scales (cf., Mehta and Lau, 1997).

b. Monsoon climate indices

A first step toward achieving a better understanding of monsoon predictability is the development of quantitative measures to characterize the ASM climate and its subsystems. This requires the construction of appropriate measures of different and closely related aspects of monsoon climate. Up to now, there have been several monsoon indices that are commonly used for the ASM based either on rainfall or circulation (Mooley and Parthasarathy 1984, Webster and Yang 1992, Shen and Lau 1995, Goswami et al. 1998, Ailikun and Yasunari 1998). Most of these indices are developed based on different considerations including data availability, dynamical consistency and regional relevance. In the following, we summarize the main attributes that need to be considered for a monsoon climate index in the context of the aforementioned paradigm. They are:

- Representativeness of the annual as well as variability (interannual or longer) of the ASM including its subcomponents;
- Relevance in regional (geographical, because of society impacts) as well as global context

- Simplicity for construction, preferably from direct observables such as rainfall, wind, temperature or moisture;
- Internal dynamical consistency, if different parameters are used;
- Robustness and reproducibility by different data sets (for the same variables), and
- Expandability to include long-term, multi-decadal time scales

Obviously, because of practical constraints, not all the conditions can be met. In this paper, we have considered them to the extent possible, in the development of monsoon indices and the descriptions based on them.

3. Data description

To establish the monsoon rainfall climatology and variability, we used 18 years (1979-1996) of global rainfall estimate from the CPC Merged Analysis of Precipitation (CMAP) (Xie and Arkin 1997). This data set is derived from multiple information sources including gauge observations, estimates inferred from a variety of satellite infrared and microwave observations, and the NCEP-NCAR (National Center for Environmental Predictions/ National Atmospheric Research Center) reanalyses. For comparison, we have also included the Global Precipitation Climatology Project (GPCP) Version 1 combined precipitation data set (Huffman et al. 1997) and other commonly used satellite rainfall products i.e., the Microwave Sounding Unit (MSU) and the GOES Precipitation Index (GPI). The GPCP combined data set covering a period from 1987-1995 is similar to the CMAP in the data sources but differs in the treatment of the blending of the satellite and the in-situ observations. The MSU satellite rainfall has been merged with rain gauge data and the GPI is IR-based satellite-only rainfall estimate.

For development of the monsoon circulation indices and associated dynamical characteristics, we used 40 years (1958-1997) of wind reanalysis from NCEP-NCAR. This is the only multi-decadal reanalysis data set available at the time of this study. A description of the data set can be found in Kalnay et al. (1996). Other data set used included SST from NCEP and all India monsoon rainfall.

4. Regional monsoon characteristics

a. Rainfall and circulation climatologies

In this section, we describe the development of regional monsoon climate indices that will be used in subsequent analysis to characterize the climate variability of the ASM and its subcomponents. We begin with a description of the climatological rainfall and circulation fields. Even though the basic climatological features of the ASM are well known, they are shown here to provide references for later discussions. To ascertain the reliability of the CMAP rainfall, we also show the climatology of other rainfall products for comparison.

The CMAP (Fig. 2a) rainfall climatology shows clearly the broad features of monsoon precipitation over the warm pool of the Indian Ocean and the Pacific. Four monsoon rain centers, each anchored to the west side of the continental or maritime land masses, can be identified near the South China Sea/Philippines region, southern Indochina, Bay of Bengal, and the west coast of the Indian subcontinent. Climatological CMAP rainfall amounts in these regions exceed 16 mm/day, with the maximum over the Bay of Bengal in excess of 20 mm/day. These features are consistent with GPCP (Fig. 2b). The MSU (Fig. 2c) and the GPI (Fig. 2d) products yield heavier precipitation over the Bay of Bengal but less well defined signals over the other centers. The first two centers i.e., South China Sea and Indo-China appear to be linked to an extensive region of precipitation over the western Pacific Intertropical Convergence Zone (ITCZ) and to a branch of moderate rain over the East China Sea across southern Japan. This can be identified with the well-known *Mei-yu* or *Baiu* rain band. In the CMAP climatology, this monsoon rain band is very weak. It is stronger and better defined in GPCP and in MSU, but weak and almost absent in GPI. This may be due to larger proportion of warm rain in the *Mei-Yu* rain, as opposed to deep convection in the tropics, producing a different signature in the microwave and the IR-field. As a rule of thumb, rainfall algorithm more heavily weighted with microwave signals tend to have a better-defined *Mei-yu* rain field, because of the microswave signals (both emission and scattering) are derived directly from the hydrometeors, while IR signals are mostly derived from cloud top temperature.

9

Interestingly, all four rainfall products indicate that there is a region of enhanced precipitation just south of the equator over the central Indian Ocean during the peak summer months. The presence of this mid-oceanic precipitation is consistent with the upper level divergence field (see Fig. 3d later). This feature appears to be real and may be important for understanding the dynamics of the interaction between the land-based convection vs. oceanic ITCZ in this region.

Figures 3a and b show the June-July-August (JJA) 850 mb and 200 mb large-scale circulation associated with the ASM. Evident in the large scale flow is the low level inter-hemispheric gyre circulation (IGC) which is characterized by easterlies in the southern Indian Ocean (about 10° S), connected via the Somali jet to westerlies across the Indian subcontinent. This westerly flow continues on to the southwesterly flow over the South China Sea and East Asia. An interesting feature, not previously noted, is a closed cyclonic circulation over the Indian Ocean just south of the equator, between 70-90° E. This feature is dynamically consistent with the southern hemisphere mid-Indian Ocean precipitation noted in the rainfall climatologies shown in Fig. 2. Another dominant circulation pattern is the large-scale low-level anticyclonic flow associated with the Western Pacific Subtropical High (WPSH). This circulation regime features easterlies in the tropical western Pacific, northerlies from the South China Sea to central East Asia, and southwesterlies across the Korean Peninsular and southern Japan. The IGC and the WPSH are the two dominant low-level circulation regimes that control major fluctuations of the entire ASM.

At 200mb, the monsoon circulation is dominated by the Tibetan High, which has two centers one over northern Bay of Bengal and one over northern Arabian Sea. In the region from 60° E to 120° E, and from 10°N to the equator, a strong vertical shear is noted with strong upper level easterlies overlying low-level westerlies. The 200 mb vorticity field (Fig. 3c) shows that the basic state has strong negative (cyclonic) vorticity in a zonally oriented broad band across the monsoon region, with a center to the east of the Tibetan Plateau. There are strong vorticity gradients with opposite signs to the north and south of the subtropical jetstream near 40°N and 20-30°N, stretching across the whole

10

domain. The vorticity distribution, which is mainly due to the variation of the basic state zonal wind with latitude, will have important implication in determining the dynamical characteristics of anomalous monsoon circulation (See discussions in Sections 5 and 6). The 200 mb climatological divergence (Fig. 3d) has maximum centers over the Bay of Bengal, the eastern Arabia Sea, the South China Sea as well as over the equatorial Indian Ocean. These are in agreement with the precipitation centers noted in Fig. 2. The results provide further reassurance that the NCEP wind fields and the satellite rainfall fields are dynamically consistent.

b. Monsoon indices

As discussed above, the ASM precipitation centers are strongly controlled by two large scale low level circulation systems, i.e., the IGC and the WPSH. In the following, we use the rainfall averaged over the areas (10° N -30° N, 70° E $- 100^{\circ}$ E) and (5° N $- 25^{\circ}$ N, 110° E-130° E) as a starting point for studying monsoon climate variability governed by these two circulation systems. We have experimented with different box sizes used in defining the monsoon rainfall indices. We found that provided the major climatological convective centers are included, the results are not very sensitive to the choice of box size. In the following, the JJA rainfall time series over the above regions are denoted by P_{SA} and P_{SEA}, respectively, where SA stands for South Asia and SEA for Southeast Asia. It is important to note that for example, in our definition of South Asia rainfall, the convection over the Bay of Bengal is included, in addition to that over the land region of the Indian subcontinent. For Southeast Asia rainfall, the averaging domain covers South China Sea/western Pacific and Indo-China. As we shall show later, the two areas represent distinct source regions of monsoon variability over South Asia, Southeast/ East Asia respectively. Table 1 shows that the P_{SA} is significantly correlated too AIMR with correlation of 0.43. The main difference between P_{SA} and AIMR is due to the inclusion of the Bay of Bengal which should be considered as part of the South Asia monsoon subsystem. P_{SEA} is uncorrelated with either AIMR or P_{SA}, indicating a distinct rainfall regime. When the rainfall is averaged over both the P_{SA} and the P_{SEA} domains, it has a higher correlation with P_{SEA} than P_{SA}.

11

Because reliable rainfall data over the oceanic regions do not exist before the era of reliable satellite data, it is necessary to find complementary circulation indices the same regional information contained in P_{SA} $_{SEA}$. Furthermore, it is desirable to extend the monsoon indices back in time to study possible long-term variations of monsoon dynamical characteristics. To identify circulation features that are most strongly correlated with P_{SA} and P_{SEA}, we have computed one-point correlation maps of the anomalous (with seasonal cycle removed) zonal wind, meridional wind and associated wind shears with P_{SA} and P_{SEA} respectively. For convenience, only fields that are used in the subsequent definition of monsoon circulation indices will be shown. These fields display the most coherent and well-defined features associated with each of the rainfall time series. Figure 4a shows the one-point correlation of the meridional wind shear ($v_{850 mb}$ - $v_{200 mb}$) with P_{SEA}. The most prominent feature is a large area of positive shear signaling a direct meridional circulation with low level poleward and upper level equatorward flow over the Indian subcontinent. Coupled to this meridional circulation is a reversal meridional circulation over northern China and the western Pacific east of the Philippines. In contrast to P_{SA} , the most well-defined feature correlated with P_{SEA} is an alternation of upper level easterly and westerly wind in the longitudinal sector from 110 °E to 150° E (Fig. 4b). In the extratropics, the zonal regimes span the entire Eurasian sector, with a secondary maximum northwest of the Himalayas. The association of the East Asian upper level jet with tropical convection over the East Asian sectors has been noted in a number of previous studies (e.g., Lau and Li 1984, Liang and Wang (1998). Based on the correlation maps shown in Figs. 4a and b, we define two regional monsoon (RM) circulation indices as:

$$RM1 = (v_{850 mb} - v_{200 mb})$$
over the region [10° N – 35° N, 70° E – 110° E,] (1)

$$RM2 = (u_{200 mb} [40° N -50° N, 110° E-150° E]$$
$$- u_{200mb} [25° N- 35° N, 110°-150° E])$$

(2)

12

where the zonal and meridional winds are averaged over the geographic regions indicated. Based on the NCEP reanalysis, the above indices have a record length of 40 years, thus permitting a reasonable statistical estimate of ASM variability. We should point out that RM1 is almost identical to the monsoon index proposed by Goswami et al. (1998). However, both RM1 and RM2 are significantly different from the monsoon index used by Webster and Yang (1992, hereafter referred to as WY). Table 2 shows a preliminary comparison of RM1, RM2 and WY with respect to P_{SA} and P_{SEA}. A more detailed comparison will be provided in Section 6. By design, the correlation of RM1 to P_{SA} (=0.64) and RM2 to P_{SEA} (=0.74) are highly significant at the 99% confidence level. It is important to note that the cross-correlation between the regional indices and the rainfall time series are very small , confirming that the indices P_{SA}/RM1 and P_{SEA} /RM2 indeed represent distinct regional and dynamical phenomena. The regional context of the monsoon indices is supported by the significant correlation (=0.53) between RM1 and the AIMR, while there is negligible correlation (=0.13) between RM2 and AIMR. Note also that the WY index has only poor correlation with AIMR (=0.24) and P_{SA} (= 0.18), respectively. This means that WY is not a good regional index for the Indian monsoon and Bay of Bengal rainfall variability. On the other hand, the WY index appears to be better correlated with rainfall anomalies summed over the South China Sea and western Pacific region P_{SEA+SA}. This is consistent with the recent findings of Aikilun and Yasunari (1998). Further comparison of RM1, RM2 and WY will be presented in Section 7.

5. Dynamical characteristics

This section is devoted to a more detailed description of the dynamical characteristics of the two monsoon subsystems, i.e., the South Asian monsoon and the Southeast/East Asian monsoon as depicted by RM1 and RM2.

a. The South Asian monsoon (SAM)

To illustrate the regional context of RM1, the correlation map of RM1 with precipitation anomalies at every grid point in the ASM region is shown in Fig. 5a. As expected, the areas of largest positive rainfall anomalies are found over South Asia,

13

including the Indian subcontinent, the Bay of Bengal, northern Indo-China and southern East Asia. Negative rainfall anomalies are found surrounding the positive rainfall center. The strongest negative anomalies are found over the southeastern Indian Ocean, the South China Sea, and the subtropical and tropical western Pacific. Associated with the positive rainfall anomalies are strong low-level westerly and southwesterly flow over the Arabian Sea and the Bay of Bengal (Fig. 6a). Two branches of cross-equatorial flow can be identified: one along the east coast of Africa and a second one from southeastern Indian Ocean. The latter appears to be the main supply of the low-level inflow into the Bay of Bengal. At the upper level, a prominent anticyclone center is found to the northwest of the positive heating (see Fig. 6b). The upper level equatorward flow is very prominent. This pattern can be identified with induced Rossby-type circulation by latent heating located off the equator (Gill 1981, Lau and Lim 1982).

The above-mentioned circulation features are linked to well-defined low-level anticyclone circulation over the coastal region of East Asia. This anticyclone represents an enhancement and eastward extension of the WPSH, which is associated with surface easterlies and subsidence over the South China Sea region (see discussion in next section). Figure 6b also shows an upper level anticyclone located to the northeast of the low-level anticyclone, directly over northern Korea, 40°N, 120°E. As we shall demonstrate later, the dynamics of the anomalous circulation over this region is underpinned by barotropic interaction with the climatological westerly jet.

Focusing back on the sector over the Indian subcontinent, Fig. 7 shows the meridional vertical cross-sections of the covariance of zonal, meridional wind, and vertical motion fields associated with RM1, averaged between the longitudes 80-90° E. The zonal wind cross-section indicates a pattern of upper easterlies coupled to a pattern of low level westerlies over the main ASM region (10-20° N). Poleward of this region, the zonal wind perturbation appears to be mostly barotropic. The strongest signal of RM1 is found in the meridional circulation field (Fig. 7b). Here, a strong negative (equatorward) meridional flow coupled to middle-to low level poleward flow is evident. Over the southern hemisphere, the meridional wind direction is reversed and much reduced in

14

scope. The meridional winds are a part of the main branch of the local Hadley circulation which spawns large scale ascending motion over the South Asian region (10-25° N) and descending motion at 30-40° N and 10°S – 0°N.

In summary, RM1 portraits a "classical" monsoon circulation system associated with latent heating over the Indian subcontinent and adjacent oceans including the Bay of Bengal. RM1 also depicts significant precipitation and circulation anomalies in the East Asia/South East Asian regions suggesting that the two monsoon subsystems are dynamically linked.

b. The Southeast -East Asia monsoon (SEAM)

The regional context of RM2 is shown in the one-point correlation map of precipitation with RM2 in Fig. 5b. In contrast to RM1, the precipitation pattern shows east-west banded structure, indicating alternate dry and wet conditions over the western Pacific and East Asia, with very weak signal over the Indian subcontinent. The meridional extend of the monsoon-related rainfall anomalies is very large, spanning from the equator to 50° N. As seen in Fig. 8, the low level circulation field indicates a strong influence from the WPSH in the subtropical region. When convection is strongly developed over Southeast Asia/South China Sea region, westerly low level flow prevails from the southern Bay of Bengal to the western Pacific, across the central and southern South China Sea. At the same time, the WPSH shifts northward and eastward exerting strong influence over East Asia. The easterly inflow near 25 –30°N is associated with local sinking motion and the westerly return flow is associated rising motion near 40-50°N (see Fig. 9c). At 200 mb, the most prominent feature is the presence of an intensive anticyclone, whose main effect is to cause the axis of the climatological subtropical jet to migrate northward by about 10-15° latitude. This represents a very marked response of the subtropical upper level flow to tropical heating in the Southeast Asia region. The East Asian anticyclone is connected upstream to an anomalous anticyclone to the northwest of northern India, indicating again that the East Asian monsoon is dynamically linked to its South Asian counterpart.

15

Figure 9 shows vertical cross-sections of the covariance of the wind fields, which further illustrate the fundamental different dynamical structure of the SEAM vs. SAM. The dominant feature in the zonal wind cross-section (Fig. 9a) is a barotropic structure signaling a northward shift of the upper troposphere jet stream, which creates a strong local anomalous vorticity gradient. The shift in the zonal wind is associated with strong poleward flow just south of the zonal wind maximum (Fig. 9b). The resultant meridional flow advects basic state vorticity from the south to the north of the climatological jet while transporting momentum northwards. A more detailed comparison between the vorticity balance for SAM and SEAM will be presented in Section 5c.

In the tropical region, characteristics of the "classical" monsoon circulation such as upper level easterlies and equatorward flow as well as low level westerlies and poleward flow can still be discerned up to 20°N in Figs. 9a and b. However, the local latent heat-induced Hadley circulation appears to be squeezed into a narrow latitudinal span with rising motion centered near 20° N, and subsiding motions at 10° N and 30° N, as shown in Fig. 9c. Here, the multi-cellular structure of the meridional vertical motion field in SEAM is in stark contrast to the broad ascent for SAM. Because of the relatively smaller magnitude of the extratropical precipitation compared to the tropics, the anomalous ascent centered at 40°N is not likely to be caused by latent heating, but rather induced by meridional wind advection of vorticity associated with the northward movement of the jetstream (see also discussion in next section).

c. Vorticity balance and teleconnection

The aforementioned dynamical characteristics of SAM and SEAM are further illustrated by an examination of the vorticity balance over these regions. The major contribution to the vorticity anomaly (defined with respect to the climatological mean) at 200 mb is given by the vorticity equations:

$$\frac{\partial \zeta'}{\partial t} + \overline{\mathbf{V}} \bullet \nabla \zeta' + \mathbf{V}' \bullet \nabla \overline{\zeta} + (\overline{\zeta} + f)\nabla \bullet \mathbf{V}' + \beta \mathbf{V}' + residual = 0$$

$$(3)$$

where an over-bar represents a climatological mean and a prime denotes the anomaly

16

from the mean. The symbols have their usual meaning. The residual term represents contribution by twisting terms and by vertical motions which are not considered here.

Figure 10 shows the time series of the two most dominant terms of the vorticity equation averaged over the RM1 and RM2 domains. For RM2, both the lower latitude and higher latitude domains are included. The root-mean-square values of all terms shown in Eq (1) are shown in Table 3. The sign in front of the rms value is determined from the sign of the correlation coefficient with the most dominant term in each domain (shown in column 3 of Table 3). For the RM1 region, it can be seen from the inverse variations shown in Fig. 7 (top panel) that the major steady state vorticity balance is between the meridional advection of planetary scale vorticity and the vorticity generation by the divergence of the anomalous flow , i.e.,

$$\beta v' + (\overline{\zeta} + f)\nabla \bullet \mathbf{V}' \approx 0$$

(4)

Notice from Table 3 that there is also a close balance between the two advection terms so that the total advection effect in this region is effectively quite small.

In the RM2 region near the climatological position of the East Asia jet (Fig. 3b), the advection by the mean circulation becomes important. Table 3 shows that the major vorticity balance is shared among three terms, i.e.,

$$\beta \mathbf{V}' + (\zeta + f)\nabla \bullet \mathbf{V}' + \overline{\mathbf{V}} \bullet \nabla \zeta' \approx 0$$

(5)

Northward of the climatological jetstream position (in the northern domain of RM2 shown in Fig. 4b), Table 3 shows that the dominant balance is between the vorticity generation induced by divergence and the advection of the mean circulation, i.e.,

$$\beta \mathbf{V}' + (\zeta + f)\nabla \bullet \mathbf{V}' + \overline{\mathbf{V}} \bullet \nabla \zeta' \approx 0$$

(6)

One consequence of the different vorticity balance between SAM and SEAM is that the two regional monsoons give rise to very different teleconnection patterns. Figure 11

17

shows the one-point correlation maps of RM1 and RM2 with the 300 mb geopotential field. Areas with correlation coefficients equal to or exceeding the 95% significance level are shaded. In RM1 (Fig. 11a), the anticyclone over northwestern India due to heating over South Asia appears as a part of an elongated ridge system extending from northern Africa. The South Asia anticyclone is linked to a high over northeastern Asia,. As discussed previously, this high is associated with the fluctuation of the WPSH. The teleconnection pattern of RM2 is broadly similar to that of RM1, but much stronger and more well-defined (Fig. 11b). It indicates that fluctuation in RM2 is associated with a strong meridionally oriented trough/ridge system spanning the coastal region of East Asia, Japan and the north central Pacific. This system is apparently connected to the north-south migration of the subtropical jetstream associated with heating over the South China Sea and western Pacific region. The similarities between the RM1 and RM2 teleconnection patterns in the Asian and western Pacfic sectors, indicate that the northward shift of the jetstream and the fluctuation of the WPSH may be synchronized with the development of the South Asia High. Similar wavetrain signals are also noted over North America, downstream of the north Pacific anomalies. The fact that similar downstream teleconnection signals are excited independent of the sources suggest that they may be manifestation of intrinsic barotropic modes in the northern summer basic state flow (Lau and Peng 1992).

6. SST Relationships

As discussed in Section 2, the dynamical structure of the monsoon climate is strongly influenced by intermediate and slow processes, i.e., lower boundary condition in both the adjacent regions and in those far from the monsoon region. Whereas the largest interannual basin-scale SST anomalies (SSTA) occur during ENSO, these SSTAs are not necessarily the maximal (in the sense of providing the most sensitivity) in influencing ASM variability . For regional monsoon prediction, it is necessary frist to identify what is the geographical locations of SSTA that is most effective in causing monsoon fluctuations and then ask the question how these SSTAs relate to ENSO. In this section, we discuss the sensitivity of SSTA forcing for SAM and the SEAM.

Figure 12 shows the contemporaneous and lagged covariances of RM1 with SSTA over the Indo-Pacific region. The label MAM (DJF) indicates SST patterns one season (two seasons) preceding a positive SAM anomaly. The areas exceeding 95% significance are shaded. A strong SAM is preceded in the antecedent winter by a dipole SSTA pattern in the North Pacific with positive anomaly over the western North Pacific and negative anomaly over the eastern North Pacific. During the preceding MAM, a SSTA pattern emerges which resembles that of a La Nina with a cold tongue in the eastern equatorial Pacific, a subtropical mid-Pacific positive SSTA and a negative SSTA over the eastern North Pacific. Notice that the Arabian Sea and the Bay of Bengal have above normal SST at this time. The JJA correlation indicates that the subtropical SSTA further strengthens and becomes anchored to the East Asian continent. This movement of the SST is also consistent with the eastward shift of the subtropical high during strong SAM, as noted previously. Over the Indian Ocean, a strong SAM is associated with a simultaneous cooling of the western Indian Ocean along the coast of Somalia. This may reflect the enhanced oceanic upwelling due to increased monsoon wind. The eastern Pacific SSTA becomes quite extensive in JJA. Except for the region over the western Pacific and the Indian Ocean, the JJA SSTA projects strongly on the canonical SSTA pattern observed during ENSO.

The SST correlation with RM2 shows that the SEAM is associated with distinctly different SST anomaly patterns (Fig. 13). Enhanced convection over Southeast Asia is preceded in the previous cold season by a well-defined dipole SSTA pattern in the central subtropical Pacific, oriented in a southwest-northeast direction. In MAM, the SSTA pattern expands but remains essentially stationary. At this time, warming is noticed along the coastal region of China while overall cooling occurs in the Indian Ocean. In contrast to the SAM, the SEAM appears to be most sensitive to the mid-Pacific SSTA dipole pattern, and there is only a weak resemblance to the El Nino SST signal in equatorial western Pacific. During JJA, the maximum positive SST anomaly is locked on to the extratropics of the western Pacific, encompassing the Yellow Sea, the Sea of Japan and the central North Pacific. The cooling of the Indian Ocean has spread to cover the South China Sea and the western Pacific up to 25° N. The sharp north-south SST

19

gradient in the subtropical western Pacific appears to be coupled to the rainfall and circulation anomalies (see Fig. 5b), with warm water overlain by a dry zone and surface easterlies and the cooler water to the south, by a wet zone with surface westerlies. It is noted that while the overall SSTA pattern has some resemblance to La Nina in the eastern Pacific, areas of strongest SSTA are found over the oceans adjacent to the monsoon land masses.

The JJA correlation patterns of SST (Fig. 13c), rainfall (Fig. 5b) and circulation (Fig. 8) over the subtropical western Pacific are suggestive of strong ocean-atmosphere feedback associated with the fluctuation of the WPSH and convection over the South China Sea, i.e., P_{SEA} region. . One possible scenario is that the increased convection over the South China Sea enhances subsidence in the subtropical zone near 30-35° N resulting in cloud-free sky SST (see Fig. 10c and 6b). Increased insolation in the dry zone may lead to the rapid shoaling of the oceanic mixed layer and warming of the surface waters of subtropical western Pacific. The increased anticyclonic flow from the WPSH will bring more moisture to southern China and return drier air mass over the dry/warm water zone, thus accelerating the SST warming over that region. On the other hand, the extensive cooling of the Indian Ocean and South China Sea in JJA is likely due to the increased upwelling and surface evaporation. This differential heating and cooling of the subtropical western Pacific and the Indian Ocean/South China Sea may increase the north-south thermal contrast, inhibiting (favoring) convection over the South China Sea (western subtropical Pacific) thus providing a negative feedback on SEAM.

7. The annual cycle

In this section, we discuss additional attributes of the regional monsoon indices relevant to the present description of the ASM climate. It has been emphasized that the annual cycle is a crucial component in the consideration of interannual variability of the monsoon and ENSO. This is evident in the well-known phase-locking of the evolution of El Nino to the annual cycle. Since the monsoon is a key contributor to the annual cycle variation of the tropical ocean-atmosphere, a better understanding of the relationship between the monsoon and ENSO must be viewed in the contact of the entire

20

annual cycle.

a. Annual cycle variability

Figure 14 shows the scatter plot of RM1 and RM2 as a function of calendar months. The shaded regions mark the boundary of the bounds of the 1-σ variation for each time series. The annual variations for both indices are clear. RM1 switches sign from May to June and again from September to October. The positive values of RM1 during JJAS signal a reversal of the meridional wind from the rest of the year. In JJA, the interannual variability of RM1 is actually quite small compared to the annual amplitude. This indicates that even for the most anomalous SAM year, the course of the seasonal march of the SAM regional circulation is not significantly altered. This is an indication of the strong control of the annual cycle variation on the SAM circulation, where diabatic heating processes dominates. In contrast, during DJF, the interannual variability of RM1 is much larger than that during JJA, possibly because of the larger control by mid-latitude chaotic dynamics during boreal winter over the north of the Indian subcontinent. Figure 14b shows that the peak phase of RM2 is July through September with a maximum in August. Note that the onset (as represent by steep rise of RM2) occurs from June to July about a month later than RM1. This is in accordance with the noted discontinuous advance of the monsoon rain band, i.e., *Mei-yu* and *Baiu* over East Asia, which tend to undergo transitions in submonthly time scales. Interestingly, the interannual variability of RM2 is about the same all year round. As noted before, RM2 is strongly controlled by mid-latitude dynamics and its interaction with tropical convection is likely to occur through coupling of the subtropical jets with the divergent circulation generated by tropical convection.

b. Annual cycle-ENSO modulation

To explore the relationship between the annual cycles of the regional monsoon and the annual variation of the large scale SSTA forcing, we present the phrase portraits of the regional monsoon indices with respect to the Nino-3 SST variation in Fig. 15. In this figure, the solid curve represents the 40-year climatological annual cycle trajectory which describes the annual variations of the monsoon index and Nino-3 SST. The composite

21

annual cycles for 6 warm events and 6 cold events are also shown. The interannual variability of the monsoon index is marked by the shaded area around the annual cycle trajectory, based on one-standard deviation from the climatology. The annual cycle trajectory indicates that South Asia monsoon activity, as reflected in RM1, commences from April when the Nino-3 SST is warmest (Fig. 15a). The monsoon strength rapidly increases from May through July; reaching its peak in July, while the Nino-3 SST falls as the cold tongue develops. Note that RM1 changes sign from negative to positive between May and June signaling the establishment of the direct monsoon meridional cell with low level poleward and upper level equatorward flow over South Asia. The SAM withdraws very rapidly from August to December when the cold tongue is well developed and the Nino-3 SST remains below 25° C. The reversal of the local meridional cell which is one of the defining characteristics of SAM, can be seen in the negative extremes of RM1 in the cold season DJFM. Note that the interannual variability of RM1 is much larger during DJF compared to JJA. During warm events (dotted trajectory), the annual cycle is considerably reduced with RM1 reaching to a lower peak value in July and the annual swing in Nino-3 SST less than 1.5° C (compared to about 2.5° C in the climatological mean). In contrast, during cold events, the annual cycle (dot-dashed line) is much accentuated with a peak-to-peak swing of about 4.5° C. During cold events, RM1 is noticeably enhanced. The annual trajectories of the cold and warm events are clearly distinct from the climatological trajectory evidencing the impact of remote SSTA forcing on the course of the evolution of the regional monsoon with respect to Nino-3 SST.

For RM2 (Fig. 15b), the annual cycle variation with respect to the Nino-3 SST is similar to that of RM1. Here, the abrupt transition from negative to positive RM2 (northward jump of the subtropical jet) occurs from June to July, reaching a peak in August. This is consistent with the different stages in the development of the regional monsoon precipitation system, i.e.,Mei-yu in China, Changma in Korea, and Biau in Japan. During warm events (dotted trajectory), the annual cycle amplitude of SST is substantially reduced compared to cold events (dot-dashed trajectory). There is a small but noticeable increase of RM2 in the months of June through September from warm to cold events. A noteworthy feature is that the advance of the SEAM from April through

June appears to be delayed while the Nino-3 SST cools substantially. During cold events, the monsoon transition from June to July in RM2 is very marked.

8. Further discussions

In this section, we present results of a comparison of the basic properties of the regional monsoon indices developed in the previous sections to that of Webster and Yang index (WY). As noted before, the WY is used by many recent investigators as an index for the interannual fluctuations of the Asian summer monsoon.

a. Rainfall and circulation associated with WY

The WY monsoon index is constructed from the zonal wind shear between the 850 mb and the 200 mb wind in the region of the climatological JJA upper tropospheric easterly jet overlying low level westerlies, spanning the Indian Ocean and the western Pacific (5- 20° N, 60 – 120° E). Figure 16 shows the correlation of WY with the CMAP rainfall over the ASM region. It is obvious that WY captures aspects of both the RM1 and RM2 rainfall patterns (Figs. 6a and b). It depicts the east-west banded rainfall pattern in the western Pacific similar to RM2. It also depicts the inverse relationship between rainfall over the equatorial Indian Ocean and the Indian subcontinent. However, the Bay of Bengal and the Indian subcontinent no longer appear as a major center of action. In a broad sense, the WY appears to capture coherent large scale rainfall patterns over the western Pacific which varies inversely with that over the Indian Ocean, with mixed signal over India. The results here are in agreement with those of Goswami et al. (1998) and Ailikun and Yasunari (1998) who found that WY is not related to Indian rainfall but more to convection over the western Pacific.

The circulation pattern associated with WY is shown in Fig. 17. At 850 mb, WY is associated with an elongated band of westerly wind anomaly centered at 10° N, stretching from the east coast of Africa to the South China Sea. Also noted is a band of easterly anomaly from the dateline to 140° E, forming a convergent center near (0° N, 120-140° E). At 200 mb, WY is linked to the Tibetan Anticyclone and easterly flow over the Indian Ocean and the Arabian Sea. A downstream wavetrain pattern over East Asia and

23

Japan is also noted. The circulation pattern associated with WY is somewhat similar to that of RM1, but the spatial scale appears much larger, encompassing the entire Indian Ocean and much of the western Pacific. The SST correlation field (Fig. 18) show evolution features that resemble those of the ENSO cycle with the positive phase of WY coinciding with a cold event, and with SST anomalies concentrated along the equatorial regions of the eastern Pacific and the Indian Ocean (Fig. 18c). Comparing the associated rainfall and circulation and SST fields, WY appears to possess aspects of both RM1 and RM2, but yet lacking their regional details. Because of its emphasis on basin-scale signals along the equator, it is more appropriate to consider WY as a measure of the broad scale atmospheric circulation states of the equatorial Indo-Pacific sector.

b. Intercomparison of monsoon indices

As suggested in preceding discussions, RM1 and RM2 differ from WY in that the former two are measures of the local features of sub-components , i.e., SAM and SEAM, while WY is representative of the broad scale features. These differences are reflected in the temporal characteristics of the indices. The autocorrelation functions of RM1, RM2, WY and the Southern Oscillation Index (SOI) for different seasons are shown in Fig. 19. It is clear that RM1 and RM2 have very little seasonal memory on their own, as indicated by the rapid decline in the autocorrelation after one season (Figs. 19 a and b). This is consistent with the notion that these are regional indices in which internal dynamic plays an important role in determining their intrinsic temporal properties. On the other hand, the WY index shows a much slower decline, with significant autocorrelation up to two or three seasons. Notice both the SOI and WY suggest a hint of a "spring predictability barrier" (Webster and Yang 1992, Lau and Yang 1996). Anomalies for MAM appear to have the longest memory, remaining quite high after two seasons. For all other seasons, the memory decreases rather abruptly in passing through MAM. Thus, it appears the WY has similar temporal characteristics to the SOI and is more likely to be dependent upon the basin-scale SST variations than RM1 and RM2.

Previous studies have suggested the presence of two distinct climatic states in the monsoon-ocean-atmosphere system, the transition between them is characterized by an

intrinsic quasi-biennial time scale (Meehl 1993; Yasunari and Seki 1992, Shen and Lau 1995 and Lau and Yang 1996). It is therefore instructive to compare and contrast the three monsoon circulation indices (RM1, RM2 and WY) in such a context. Figure 20 shows the lagged correlation-longitude sections depicting the time evolution of basin scale SST along the equator in the Indo-Pacific region with respect to the three indices. A strong RM1 coincides with the developing stage of the cold phase of the equatorial eastern Pacific. The cool phase becomes fully established in DJF following a strong RM1. Since the correlation does not take into account the sign of the RM1 anomalies, the situation will be reversed for a weak RM1, i.e., weak SAM associated with the warm phase. Notice that the SST signal is stronger after than before the monsoon. This is consistent with the well-known characteristics that abnormal monsoon activities may presage and therefore could provide valuable information for predicting basin scale SST anomalies in the Pacific region (Shukla and Paolino 1982, Lau and Yang 1996). Also noteworthy is that the cold phase last from about APR (0) through APR (+1). This is in agreement with the intrinsic quasi-biennial time scales in the South Asian monsoon found in previous studies (e.g., Meehl 1997). Consistent with the discussion in previous section, Fig. 20b shows that the relationship of RM2 with basin scale SST processes is weak at best. As shown in Section 5, atmospheric activities associated with RM2 appear to be linked to a subtropical Pacific SST dipole, which appears to be, in the first order, independent of the warm and cold states in the equatorial Indo-Pacific Ocean. In contrast to RM1 and RM2, WY depicts a much tighter relationship with the equatorial basin-scale SST variations (Fig. 20c). A strong WY is closely linked to the cold phase of the equatorial Pacific Ocean with very little time lag. This is consistent with the notion of an anomalous Walker circulation which is directly linked to the variation of east-west SST gradient along the equatorial region.

c. Reproducibility and reliability

This subsection provides an assessment of the reproducibility of the monsoon indices when different data sets are used. Figure 21 shows the rainfall indices P_{SA} and P_{SEA} using the four different rainfall data sets mentioned in Section 2. In the period in which at least three of the data sets overlap (1987-1996), it can be seen that the variations of the four

25

data sets seem to agree. All indices indicate a weak SAM during 1987, 1989 and 1993 and strong SAM in 1988 and 1994. The GPI rainfall estimate is consistently the highest, while GPCP data has the lowest rainfall estimate compared to others. Except for a systematic bias of about 2 mm/day, the CMAP and GPCP variations are quite similar in both regions. Before 1987, the MSU and the CMAP differs significantly in both magnitude and variations in P_{SA} and in P_{SEA}. The MSU, being a single satellite may have suffered from problems arising from orbit changes and instrument drift during the above period (Hurrell and Trenberth 1998). This problem is significantly reduced for CMAP, because of the blending of multiple satellites and sensors (Xie and Arkin 1997). Therefore it is reasonable to assume that CMAP will have higher reliability than MSU in the period prior to 1987.

The regional monsoon circulation indices RM1 and RM2 derived from the NCEP, ECMWF, and GEOS for the overlapping period from 1980 to 1994 are shown in Fig. 22a and b respectively. For RM1, the NCEP and ECMWF agree reasonably well overall. The differences between the two data sets appear to be larger before 1984. The GEOS index agrees more with ECMWF for the entire period, but with a negative bias of about 2 m/s. Since a large portion of the meridional wind shear in RM1 may be due to the divergence component, it may be the reason for the noted discrepancies among the reanalyses. Hence the results for RM1 may be somewhat dependent on the data set used. On the other hand, Fig. 22b shows that RM2 has a robust and consistent variation among the three data sets, indicating that it is a reliable index independent of the data sources. For WY, the indices are also quite reproducible by all three data sets, even though ECMWF appears to be consistent underestimate the magnitude by about 2 m/s (Fig. 22c).

9. Conclusions

We have provided a description of the internal dynamics and boundary forcing characteristics of two major subcomponents, i.e., the South Asian and the Southeast-East Asian components of the ASM based on two sets of regional monsoon indices. These regional indices provide a distinctive description of the annual cycle and the interannual variability associated with the South Asian monsoon (P_{SA}/RM1) and the Southeast-East

26

Asian monsoon (P_{SEA}/RM2), respectively. The dynamical characteristics of the regional monsoon indices and their sensitivities to SST anomalies are compared and contrasted to those represented by the broad scale circulation index of WY.

The dynamical characteristics embodied by the regional monsoon indices are shown in Fig. 23. P_{SA}/RM1 describes a "classical" monsoon system where the 3-dimensional anomalous circulation pattern is primarily determined a balance between the advection of planetary vorticity and the generation of anomalous vorticity by the divergent flow induced by an off-equatorial convective heat source (Fig. 23a). On the other hand . P_{SEA}/RM2 describes a "hybrid" monsoon system characterized by multiple meridional cells over East and Southeast Asia, which span the deep tropics and midlatitudes (Fig. 23b). The extratropical extension of the meridional circulation is due to the strong interaction of the East Asian jetstream with tropical convection and extratropical disturbances. This interaction gives rise to the characteristic zonally oriented rainfall structure found over the East Asian monsoon region. In the extratropical region, the basic state circulation, advection and divergence flow all contribute to the balance of upper level anomalous vorticity. A corollary to the strong influence of extratropical dynamics in SEAM is the exctation of stronger teleconnection to regions outside of the ASM by the SEAM compared to the SAM. In contrast, the WY index appears to be a description of the large scale Walker circulation over the entire Indo-Pacific basin, in which the ASM large scale circulation is an integral part (Fig. 23c). However, WY does not seem to correlate well with regional monsoon rainfall variability over SAM nor SEAM. These findings are consistent with those recently reported by Goswami et al. (1988) and Aikilun and Yasunari (1988).

Our results indicate that the regional monsoon variability is governed not only by basin-scale ENSO scale related SST anomalies associated with the "slow" subsystem, but also by SSTA in the adjacent oceans within the "intermediate" subsystem. For SAM, while the influence of ENSO-related SSTA in the equatorial eastern Pacific appears to be statistically significant, the boreal spring warming in the northern Arabian Sea and subtropical western Pacific may also play a role in foreshadowing a strong SAM. For

SEAM, interannual variability is strongly tied to SSTA over the Sea of Japan, East China Sea and the South China Sea region. A strong SSTA dipole pattern with warming (cooling) in the subtropical central (eastern) Pacific during the previous spring and winter (MAM and DJF) presage a strong SEAM. However, the summertime East Asian jet variability as represented by RM2 is found to have only weak or marginal relationship with ENSO-related SSTA. However this does not preclude a strong relationship of the East Asian jet with ENSO-related SSTA during northern winter (Liang and Wang 1998). We must also note that since monsoon-ENSO relationship tends to fluctuate with decadal time scales, the above relationships are valid only for the period of the present analysis (1958-1997). Regardless, our results show that coupling of SSTA in the adjacent oceans to monsoon processes may be the key to enhancing predictability of the Asian summer monsoon. This regional coupling should be more fully exploited .

Table 1a: Cross-Correlation of PSA, PSEA and AIMR.
Correlation exceeding 99% (95%) significance
are bold faced (bracketed).

	AIMR	P_{SA}	P_{SEA}	P_{SEA+SA}
AIMR	1.00	**0.48**	0.06	0.31
P_{SA}		1.00	0.03	**0.62**
P_{SEA}			1.00	**0.80**
P_{SEA+SA}				1.00

Table 2: Same as in Table 1 except for correlation
among AIMR, RM1, RM2 and WY.

	RM1	RM2	WY
AIMR	(0.53)	0.13	0.24
P_{SA}	**0.63**	0.01	0.18
P_{SEA}	0.03	**0.74**	0.42
P_{SEA+SA}	0.41	**0.59**	**0.44**

Table 3 Root-mean-square values of major terms contributing to the 200mb vorticity balance in Eq (3) in different regions (see text for explanation). The sign of the correlation of each term with respect to the planetary vorticity balance (vβ) is shown inside a bracket to indicate the sense of the balance.

	$v'\beta$	$(\zeta+f)\nabla \cdot V'$	$V \cdot \nabla \zeta'$	$V' \cdot \nabla \zeta$	Residual
70E−110E, 10N−30N	(+)0.093	(−)0.083	(+)0.051	(−)0.054	(−)0.072
110E−150E, 40N−50N	(+)0.161	(+)0.173	(−)0.336	(+)0.087	(−)0.177
110E−150E, 25N−35N	(+)0.144	(+)0.495	(−)0.485	(+)0.118	(−)0.402

References

Ailikun, B., and T. Yasunari, 1998: On the two indices of Asian summer monsoon variability and their implications. Part I: the composite of two indices in summer. *J. Meteor.Soc. Japan* (submitted).

Goswami, B. N., V. Krishnamurthy and H. Annamalai, 1998: A broad scale circulation index for the interannual variability of the Indian summer monsoon. *Quart. J. Roy. Meteor. Soc* (submitted).

Gu, D., and S. G. H. Philander, 1995: Secular changes of annual and interannual variability in the tropics during the past century, *J. Climate*, **8**, 864-876.

Huffman, G., R. Adler, P. Arkin, A. Chang, R. Ferraro, A. Gruber, J. Janowiak, A. McNab, R. Rudolf and U. Schneider, 1997: The Global Precipitation Climatology Project (GPCP) combined precipitation dataset. *Bull. Amer. Meteor. Soc.*, **78**, 5-20.

Hurrell, J. Q., and K. E. Trenberth, 1992: An evaluation of monthly mean MSU and ECMWF global atmospheric temperatures for monitoring climate. *J. Climate*, **5**, 1424-1440.

Ju, J., and J. Slingo, 1995: The Asian summer monsoon and ENSO. *Quart. J. Roy Meteor. Soc.*, **121**, 1133-1168.

Kalnay, E., M. Kanamitsu, R. Kistler, W. Collins, D. Deaven, L. Gandin, M. Iredell, S. Saha, G. White, J. Woollen, Y. Zhu, M. Chelliah, W. Ebisuzaki, W. Higgins, J. Janowiak, K. C. Mo, C. Ropelewski, J. Wang, A. Leetmaa, R. Reynolds, R. Jenne and Dennis Joseph, 1996: The NCEP/NCAR 40-year reanalysis Project. *Bull. Amer. Meteor. Soc.*, **77**, 437-471.

Krishnamurti, T. N. , 1985: Summer monsoon experiment - a review. *Mon. Wea. Rev.*, 113, 1590-1626.

Lau, K-M., and W. Bua, 1998: Mechanism of monsoon-Southern Oscillation coupling: insights from GCM experiments. *Climate Dynamics* (in press).

Lau, K. -M., and S. Yang, 1996: The Asian monsoon and the predictability of the tropical ocean-atmosphere system. *Quart. J. Roy. Meteor. Soc.*, **122,** 945-957.

Lau, K. M., and M. T. Li , 1984: The monsoon of East Asia and its global associations - a survey, *Bull. Amer. Meteor. Soc.*, **65**, 114-125.

Liang, X.-Z. and W. C. Wang, 1998: Associations between China monsoon rainfall and tropospheric jets. *Quart. J. Royal Meteor. Soc.* **124**, (in press).

Liu, Z., and B. Huang, 1997: A coupled theory of tropical climatology: Warm pool, cold tongue, and Walker circulation. *J. Climate*, **10**, 1662-1679.

Meehl, G. A., 1997: The South Asian monsoon and the tropospheric biennial oscillation. *J. Climate.*, **10**, 1921-1943.

Mehta, V., and K. -M. Lau, 1997: Influence of solar irradiance on the Indian monsoon-ENSO relationship at decadal-multidecadal time scales. *Geophys. Res. Letters,* **24**, 159-162.

Mooley, D. A., B. Parthasarathy , 1984: Fluctuation in all india summer monsoon rainfall during 1871-1978, *Climate Change,* **6**, 287-301.

Nitta, T., and Z. Hu, 1996: Summer climate variability in China and its association with 500 hpa height and tropical convection. *J. Meteor. Soc. Japan,* **74,** 425-445.

Palmer, T. N. 1994: Chaos and predictability in forecasting the monsoons. *Proc. Indian Natn. Sci. Acad.*, **60**, 57-66.

Parthasarathy, B., R. R. Kumar and D. R. Kothawale, 1992: Indian summer monsoon rainfall indices, 1871-1990. *Meteor. Mag.,* **121**, 174-186.

Rasmusson, E. M, and T. H. Carpenter, 1983: The relationship between eastern equatorial Pacific seas surface temperature and rainfall over India and Sri Lanka. *Mon. Wea. Rev.,* **111,** 517-528.

Ropelewski, C., and J. Halpert, 1988: global and regional precipitation pattern associated with the El Nino southern Oscillation. *Mon. Wea. Rev.,* 115, 1606-1626.

Shen, S.-H., and K. M. Lau, 1995: Biennial oscillation associated with the East Asian summer monsoon and tropical sa surface temperature *J. Meteor. Soc. Japan,* **73,** 105-124.

Shukla. J., 1984: Predictability of time averages, Part II: The influence of boundary focing. Problems and prospects in long and medium range weather forecasting. Ed: D. M. Burridge and E. Kallen, Springer-Verlag, pp. 115-206.

Webster, P. J. and S. Yang, 1992: Monsoon and ENSO: Selectively interactive systems, *Quart. J. Roy. Meteor. Soc.,* **118,** 877-926.

Webster, P. J., T. Palmer, M. Yanai, V. Magana, J. Shukla and T. Yasunari, 1998: Monsoons: Processes and predictability and prospect for prediction. *J. Geophys. Res.* Special Issues (in press).

Weng, H., K. –M. Lau and Y.-K. Xue, 1998: Long-term variability of summer rainfall over China and its possible link to global sea surface temperature variability. *J. Meteor. Soc. Japan* (submitted).

Xie, P., and P. A. Arkin, 1997: Global precipitation: a 17-year monthly analysis based on gauge observations, satellite estimates and numerical model outputs. *Bull. Am. Meteor. Soc.* **78,** 2539-2558.

Yasunari, T., and Y. Seki, 1992: Role of the Asian monsoon on the interannual variability of the global climate system. *J. Meteor. Soc. Japan,* **70,** 177-189.

Figure Captions

Figure 1 Schematic indicating the various components of a monsoon-centric climate system

Figure 2 Monsoon rainfall climatology based on a) CMAP, b) GPCP, c) MSU and d) GPI. Units are in mm/day. Contour interval is 2mm/day. Areas with rain rate exceeding 6 mm/day are shaded.

Figure 3 Climatology of the Asian monsoon circulation, a) 850mb streamline, b) 200 mb streamline, c) 200 mb vorticity and d) 200mb divergence. Units and contourn intervals are as indicated.

Figure 4 Correlation pattern of a) P_{SA} and 200 mb meridional wind and b) P_{SEA} and 200 mb zonal wind. Boxes indicate regions where the averaged values of the winds are taken to construct the monsoon circulation indices, RM1 and RM2. See text for detailed explanation. Contour interval is 0.2. Areas with correlation exceeding the 95% significance are shaded.

Figure 5 Spatial distribution of covariance of CMAP rainfall with a) RM1 and b) RM2. Units are in mm/day per unit change in the corresponding index. Contour interval is 0.2. Areas with correlation exceeding the 95% significance are shaded.

Figure 6 Covariance pattern of RM1 with a) 850 mb wind and b) 200 mb wind. Shaded areas indicate significant level exceeding 95%. Units are in ms^{-1}.

Figure 7 Latitude-height cross-section showing covariance of RM1 with a) zonal wind, b) meridional wind, and c) vertical velocity. Contour intervals are 0.5 ms^{-1} (zonal wind), 10^{-3} mbs^{-1} (vertical velocity) and 0.1ms^{-1} (meridional wind).

Figure 8 Covariance of RM2 with a) 850 mb wind and b) 200 mb wind . Shaded areas indicate significant level exceeding 95%. Units are in ms^{-1}.

Figure 9   Latitude-height cross-section showing covariance of RM2 with a) zonal wind, b) meridional wind, and c) vertical velocity. Contour intervals are the same as Fig. 7.

Figure 10 Time series of dominant terms of the vorticity equation for 200 mb flow in a) the RM1 region, b) the subtropical region of RM2 and c) the extratropical region of RM2.

Figure 11 Correlation map showing the teleconnection pattern in the 300mb geopotential associated with a) RM1 and b) RM2.   Units are non-dimensional with a contour interval of 0.1.

Figure 12 Covariance map of RM1 (JJA) with SST for a) preceding cold season, DJF, b) preceding spring, MAM , and c) contemporaneous JJA.   Contour interval is in 0.05 °C. Shaded areas indicate significant level exceeding 95%.

Figure 13 Same as Fig. 12, except for RM2.

Figure 14 Time variation and standard deviation of a) RM1 and b) RM2 as a function of the calendar months. Units are in ms^{-1}. Shaded areas indicate the 1-σ bound.

Figure 15 Phase portrait of the annual cycles of a) RM1 vs. Nino-3 SST and b) RM2 vs. Nino –3 SST. Shaded region indicates 1-σ bound of RM1. Units are in ms^{-1} for the regional monsoon indices and ° C for SST.

Figure 16 Covariance of WY index with precipitation.   Contour interval is in 0.2 mm/day. Shaded areas indicate significant level exceeding 95%.

Figure 17 Covariance of WY with a) 850 mb wind and b) 200 mb wind.   Units are in ms $^{-1}$. Shaded areas indicate significant level exceeding 95%.

Figure 18 Covariance of WY with SST for a) preceding cold season, DJF, b) preceding spring, MAM and c) simultaneous summer, JJA. Areas which exceed the 95% significance level are shaded. Contour interval is 0.05°C.

Figure 19 Autocorrelation functions for different seasons for a) RM1, b) RM2, c) WY and d) SOI. Units are non-dimensional. The initial seasons are DJF (solid), MAM (dotted), JJA (dashed) and SON (dashed-dot).

Figure 20 Time-longitude section of lagged covariance of monsoon circulation index with basin scale SST anomalies. For a) RM1, b) RM2 and c) WY. Shaded areas indicate statistical significance exceeding 95% level.

Figure 21 Time series based on CMAP, MSU, GPCP, and GPI for the period 1979-1986 for a) the South Asia region and b) the Southeast Asia region. Units are in mm/day.

Figure 22 Time series based on reanalyses of NCEP, GEOS and ECMWF for a) RM1, b) RM2, and c) WY. Units are in ms^{-1}.

Figure 23 Schematic showing the basic dynamical underpinnings of the various monsoon indices a) the South Asia monsoon (RM1/P_{SA}), b) the Southeast/East Asian monsoon (RM2/P_{SEA}) and c) the broad scale Indo-Pacific circulation state (WY). Symbols used have their conventional meanings in meteorology.

Fig. 1

(a) CMAP (1979-1996)

(b) GPCP-SG (Jul1987-Dec1996)

(c) MSU (1980-1992)

(d) GPI (Jul1987-Dec1996)

Fig. 2

(a) Streamline at 850hPa

(b) Streamline at 200hPa

(c) Vorticity at 200hPa   (0.5x10⁻⁵ s⁻¹)

(d) Divergence at 200hPa   (1.0x10⁻⁶ s⁻¹)

Fig. 3

(a) $COR(P_{SA}, V_{850} - V_{200})$

(b) $COR(P_{SEA}, U_{200})$

Fig. 4

(a) <Prec., RM1>   COV

(b) <Prec., RM2>

Fig. 5

(a) 850hPa   COV w/ RM1

(b) 200hPa

Fig. 6

(a) U[m sec⁻¹]　　　　80°E–90°E (COV)

(b) V[m sec⁻¹]

(c) ω[mb sec⁻¹]

Fig. 7

(a) 850hPa   COV w/ RM2

60N ┤
50N ┤
40N ┤
30N ┤
20N ┤
10N ┤
EQ ┤
10S ┤
20S ┤
└──┬────┬────┬────┬────┬────┬────┬────┬──
   40E 60E 80E 100E 120E 140E 160E 180

→
1

(b) 200hPa

60N ┤
50N ┤
40N ┤
30N ┤
20N ┤
10N ┤
EQ ┤
10S ┤
20S ┤
└──┬────┬────┬────┬────┬────┬────┬────┬──
   40E 60E 80E 100E 120E 140E 160E 180

→
2

Fig. 8

Fig. 9

Fig. 10

(a) RM1　　　COR w/ H300

(b) RM2

Fig. 11

(a) DJF   COV w/ RM1

(b) MAM

(c) JJA

Fig. 12

(a) DJF COV w/ RM2

(b) MAM

(c) JJA
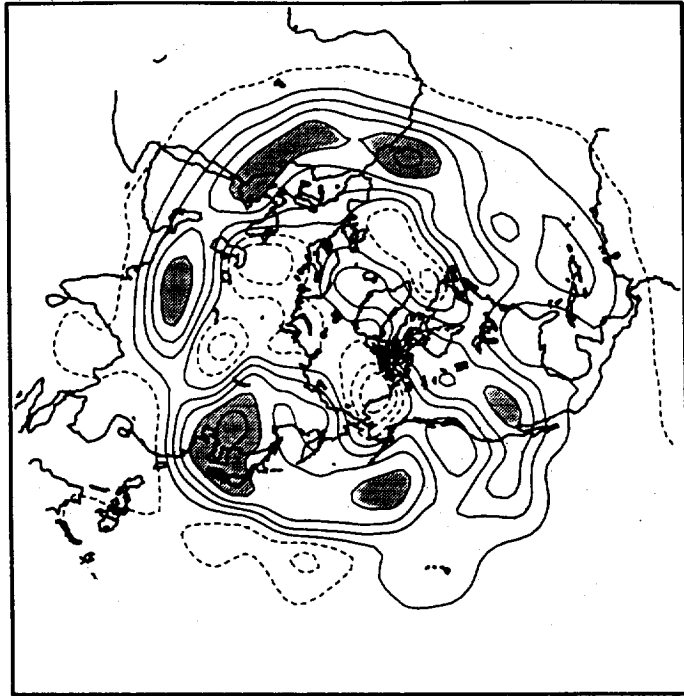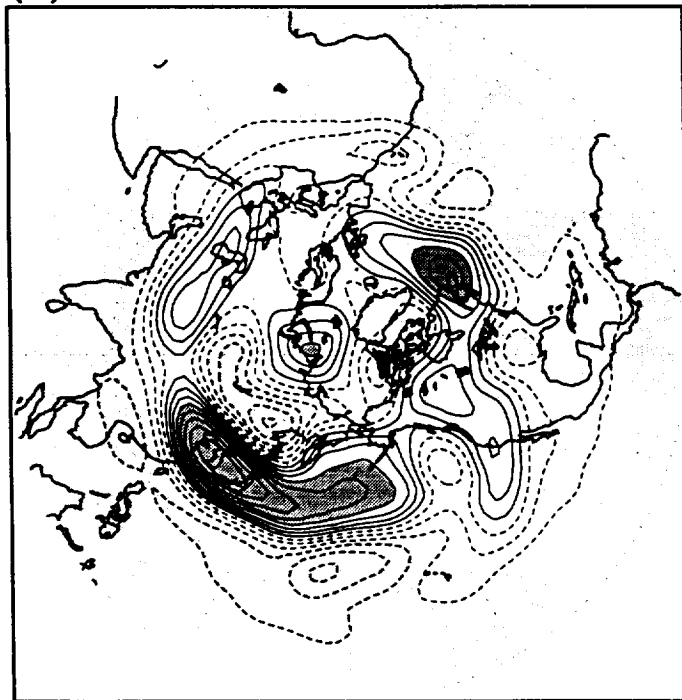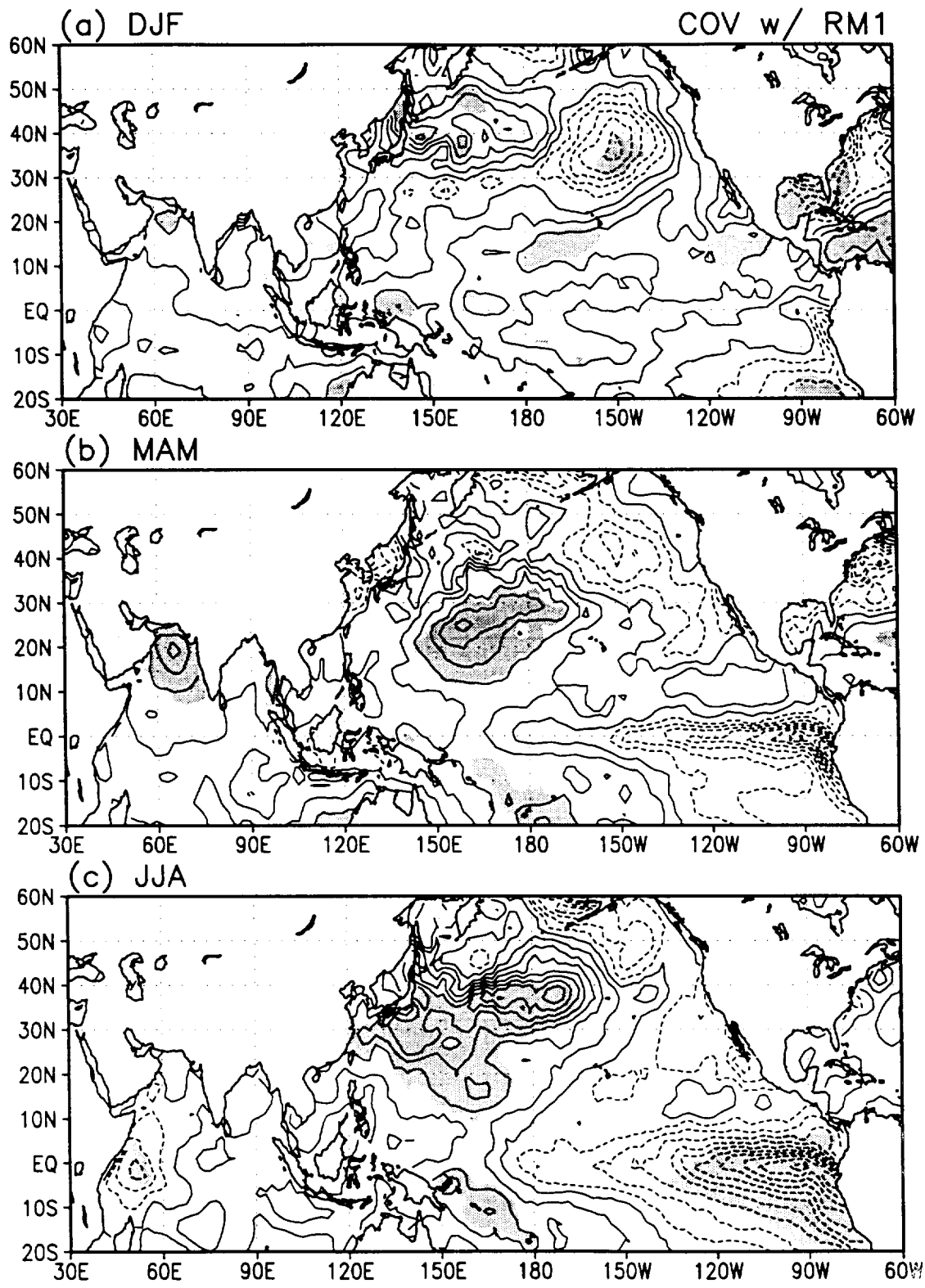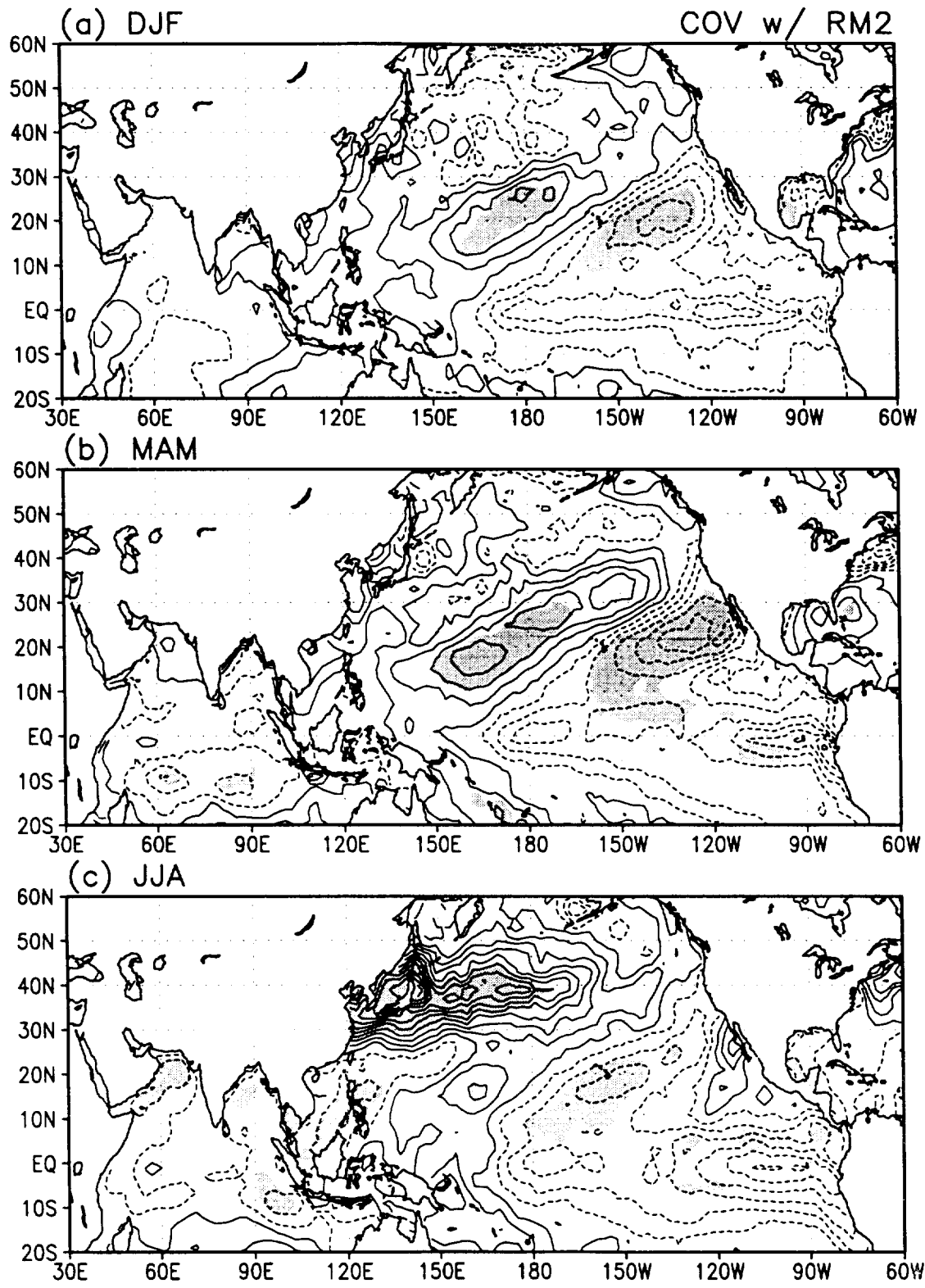
Fig. 13

(a) RM1

(b) RM2

Fig. 14

Fig. 15

<Preci., WY>   COV

Fig. 16

(a) 850hPa   COV w/ WY

(b) 200hPa

Fig. 17

(a) DJF　　　　　　　　　　　　　　　　　　　COV w/ WY

(b) MAM

(c) JJA

Fig. 18

Fig. 19

(a) RM1   (b) RM2   (c) WY   COV/EQ

APR(−1)
JUL(−1)
OCT(−1)
JAN(0)
APR(0)
JUL(0)
OCT(0)
JAN(+1)
APR(+1)

60E   120E   180   120W   60W
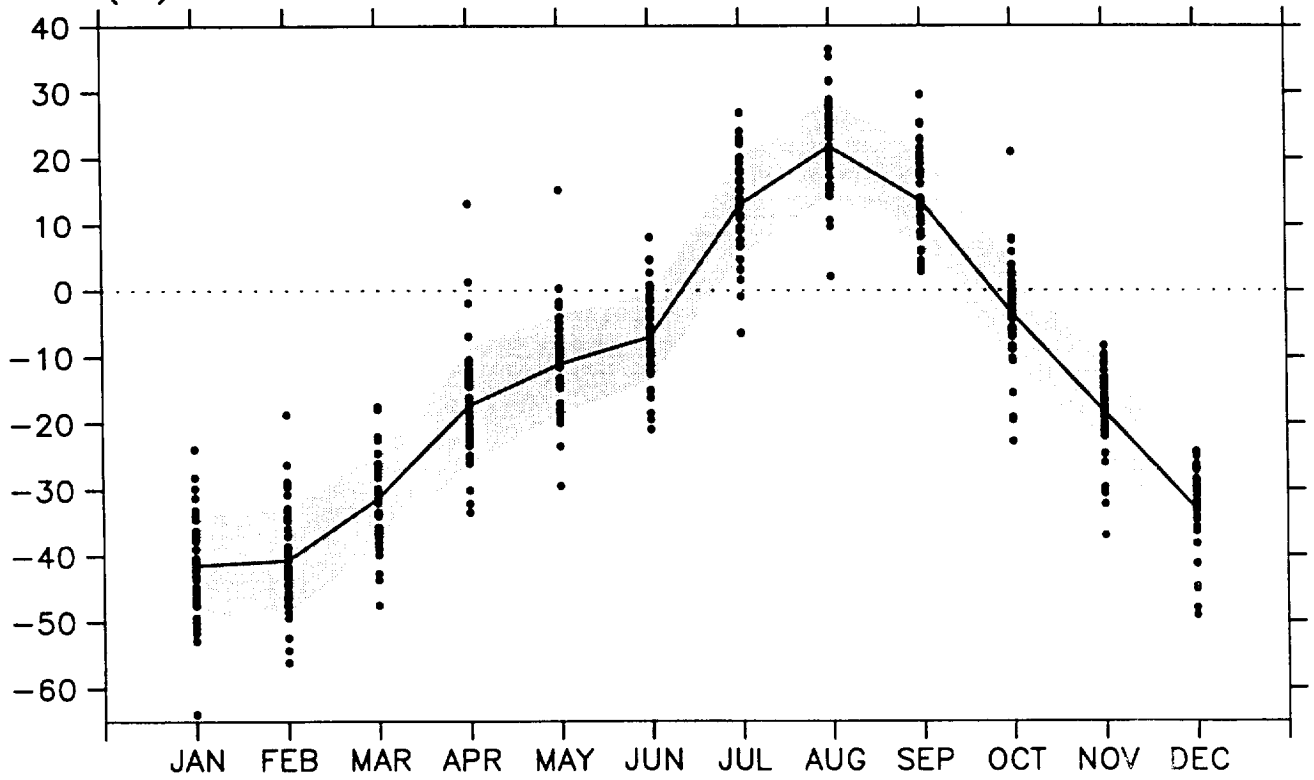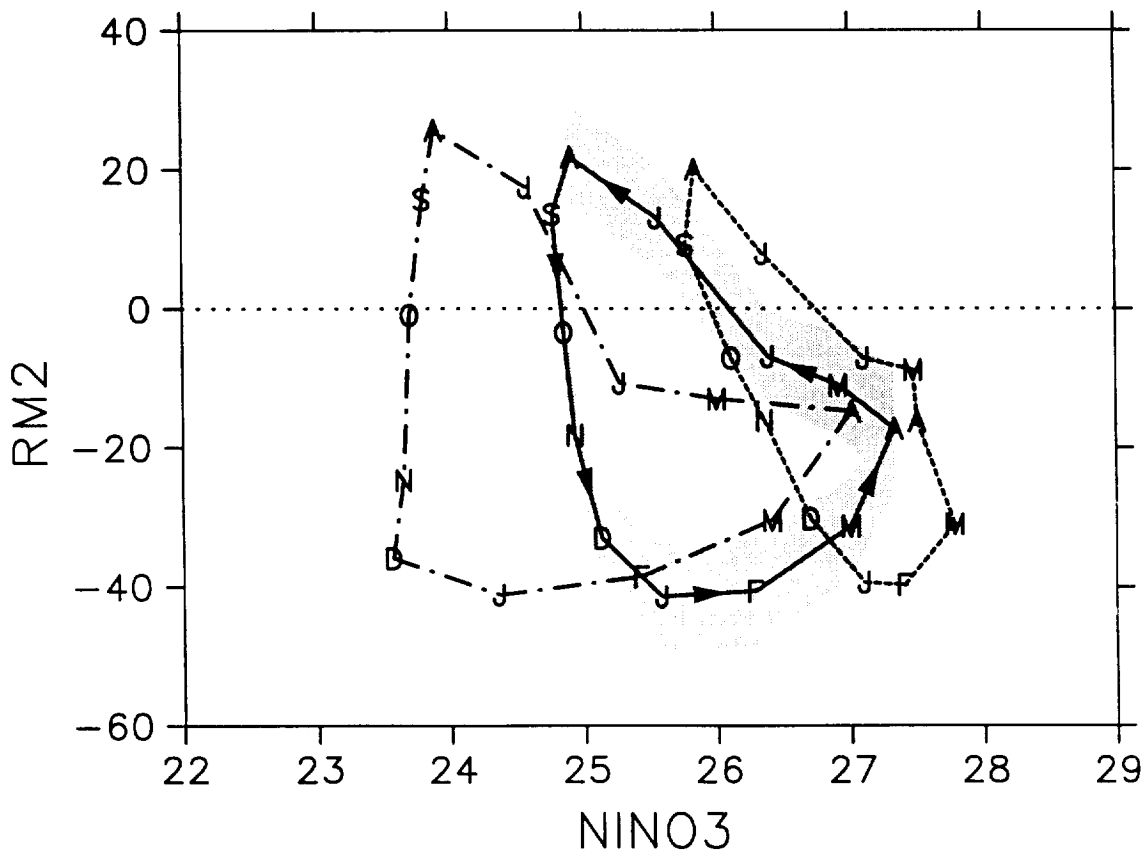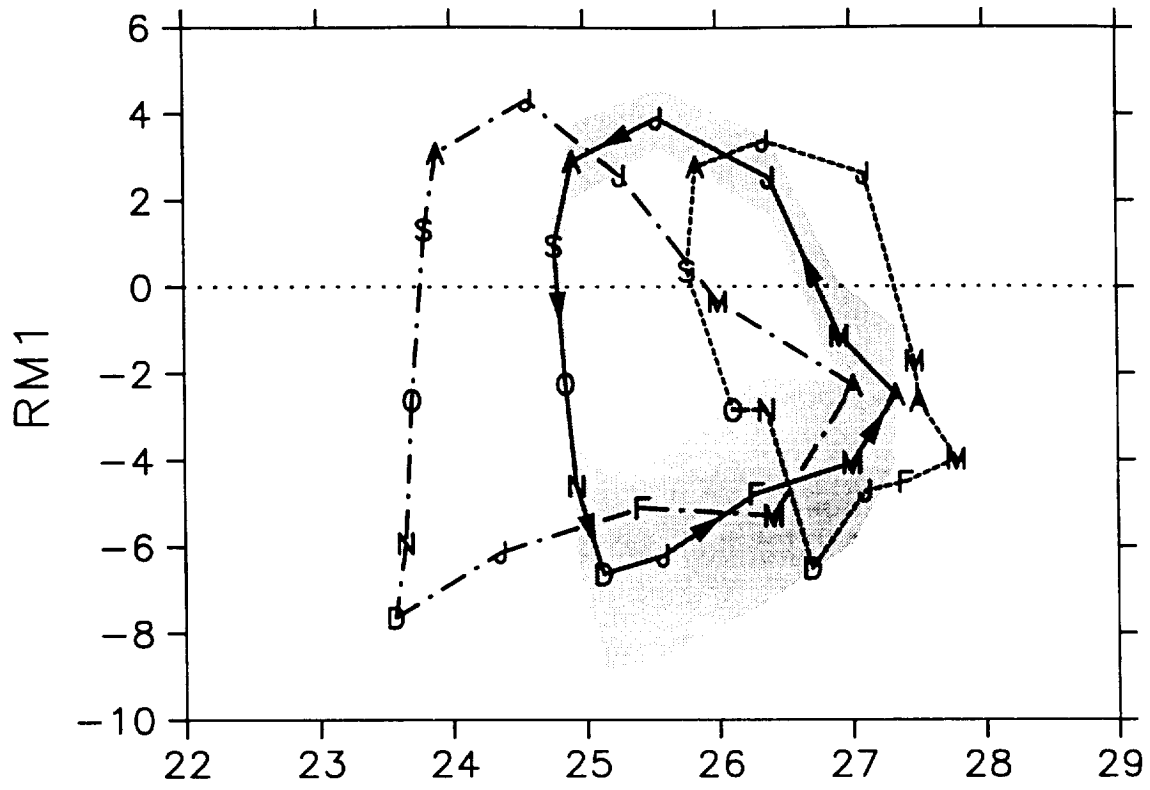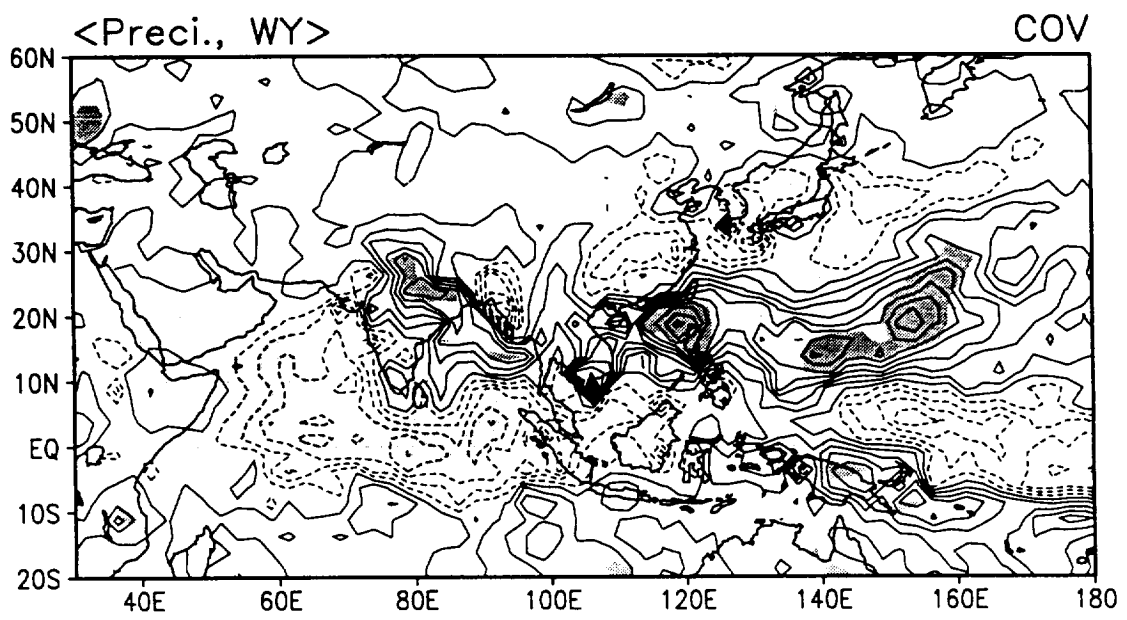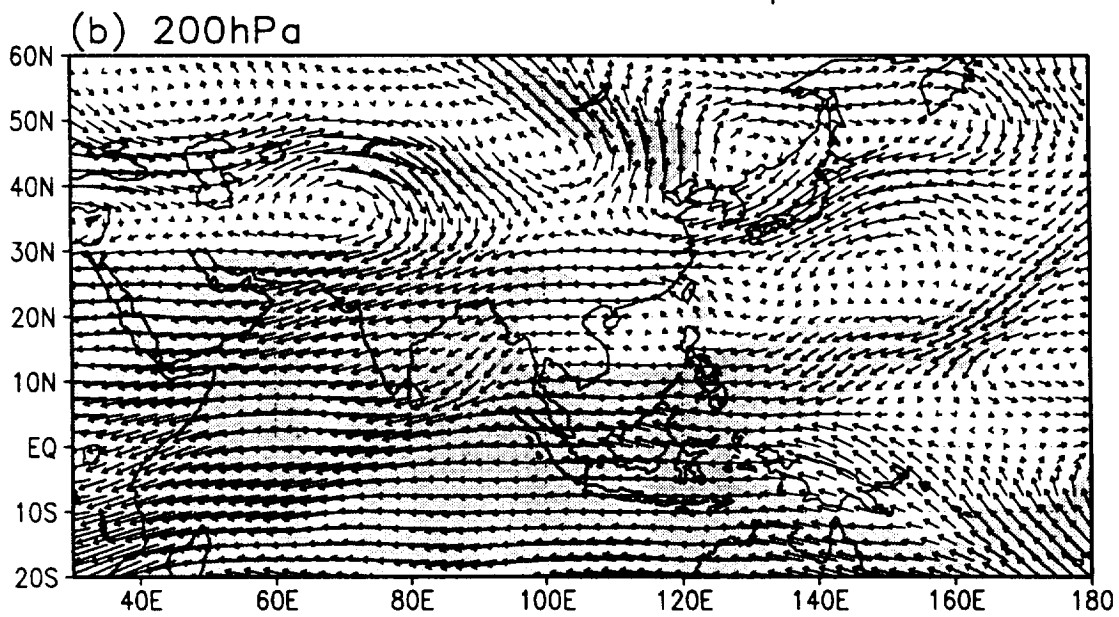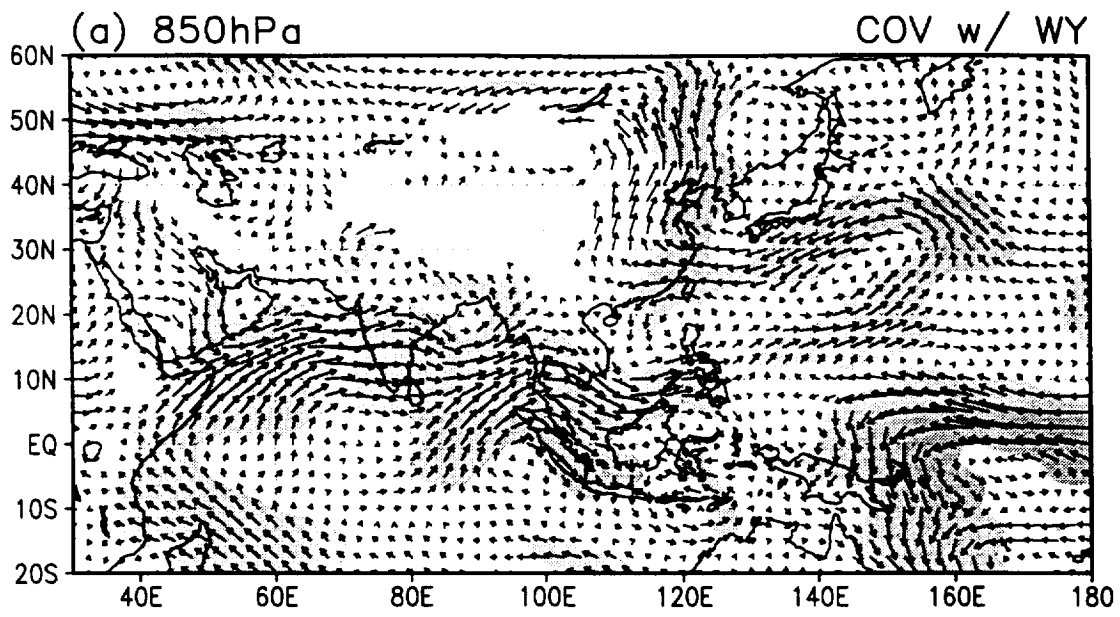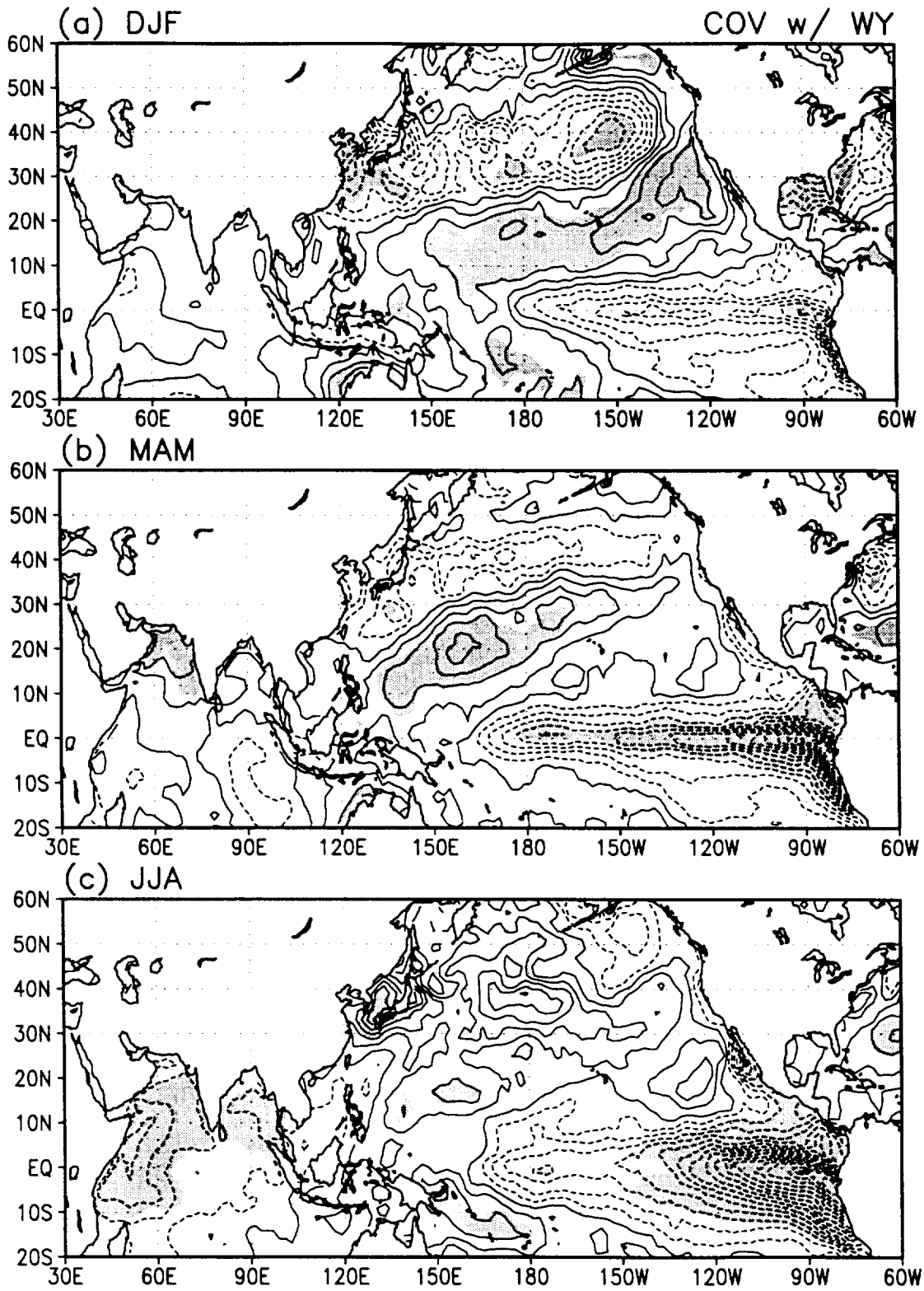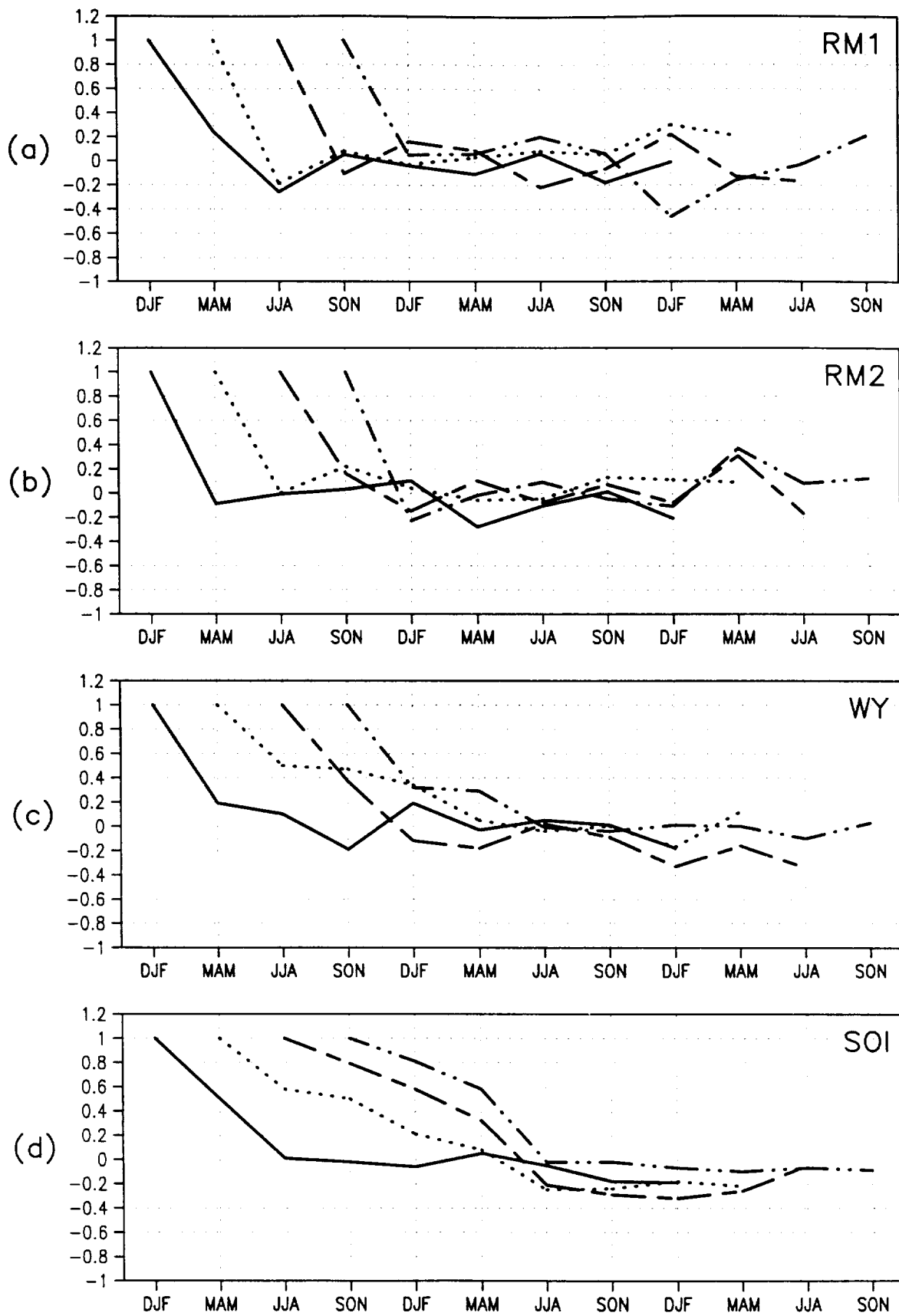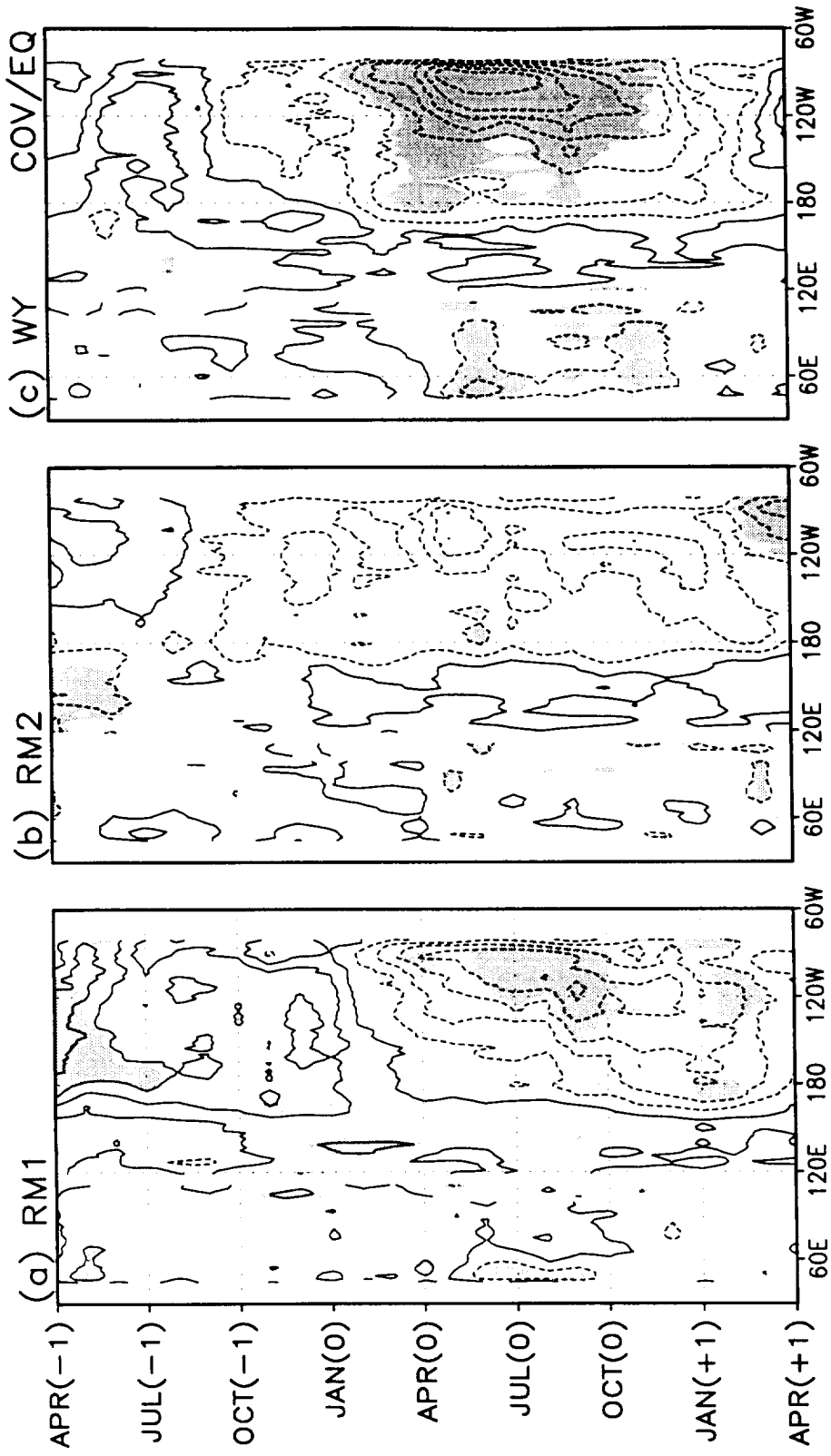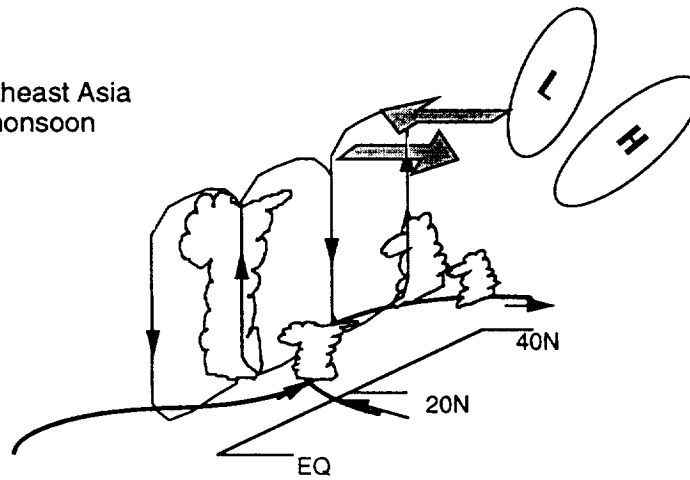
Fig. 20
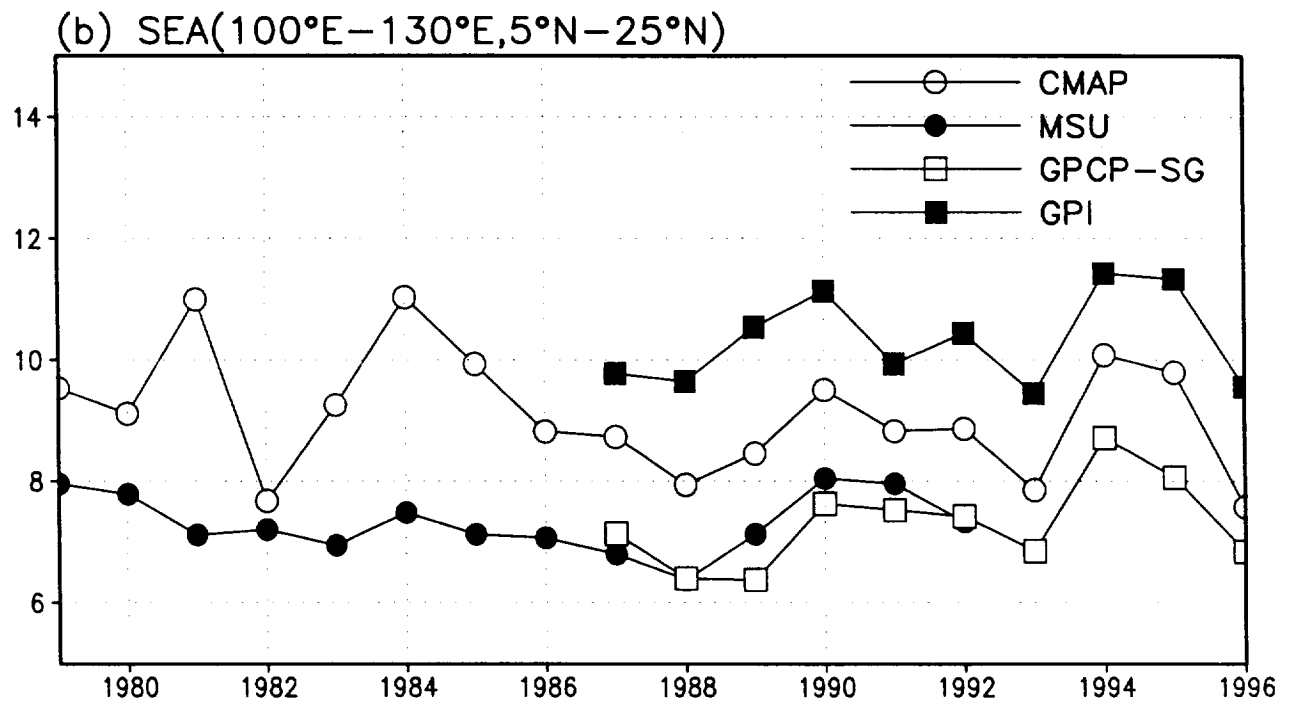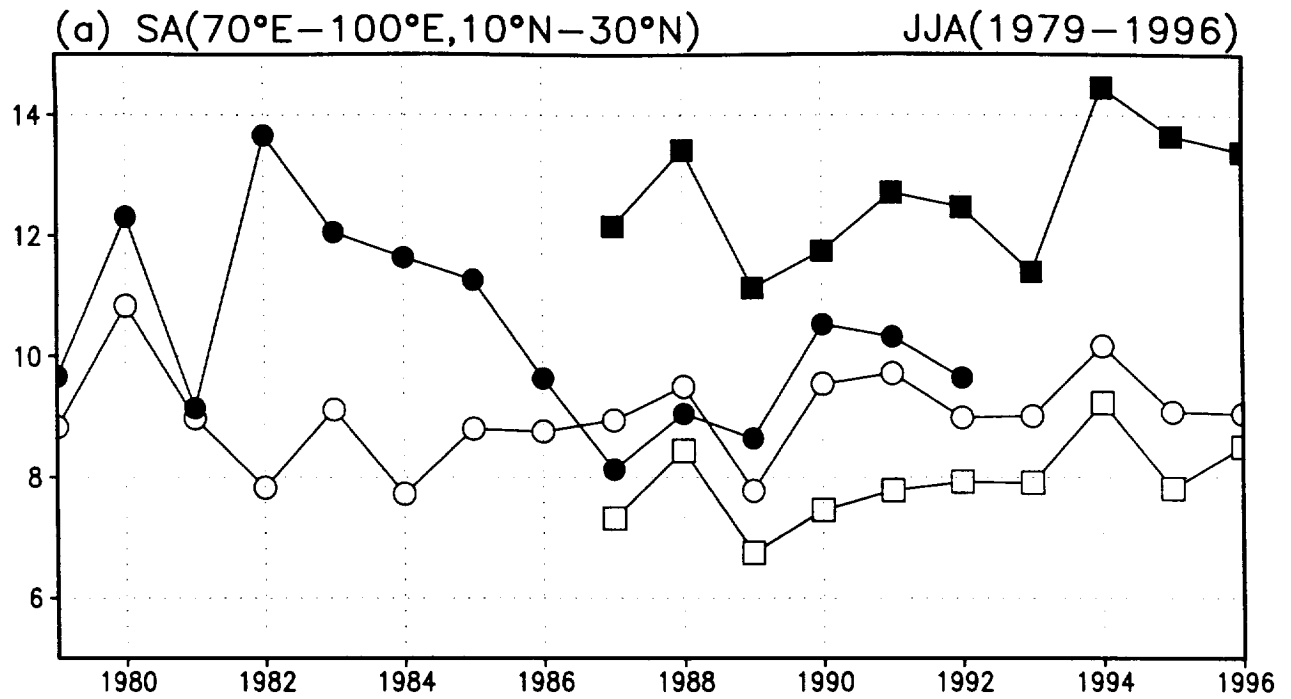
Fig. 21
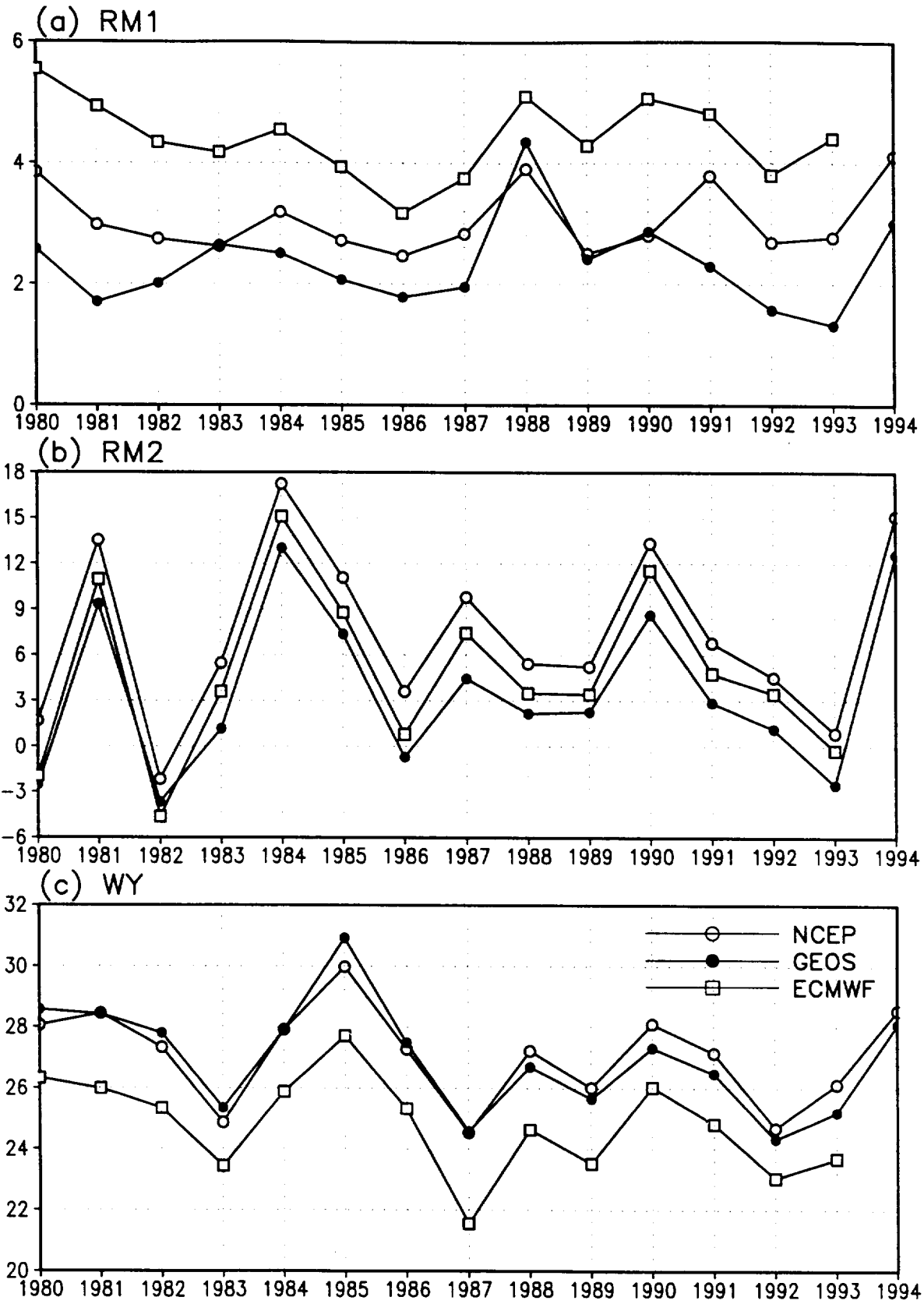
Fig. 22

a. South Asia
   RM1:Classical
   monsoon system
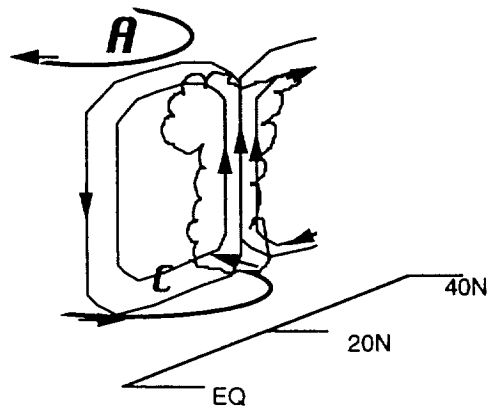
b. East Asia/Southeast Asia
   RM2: Hybrid monsoon

c. Indo-Pacific region
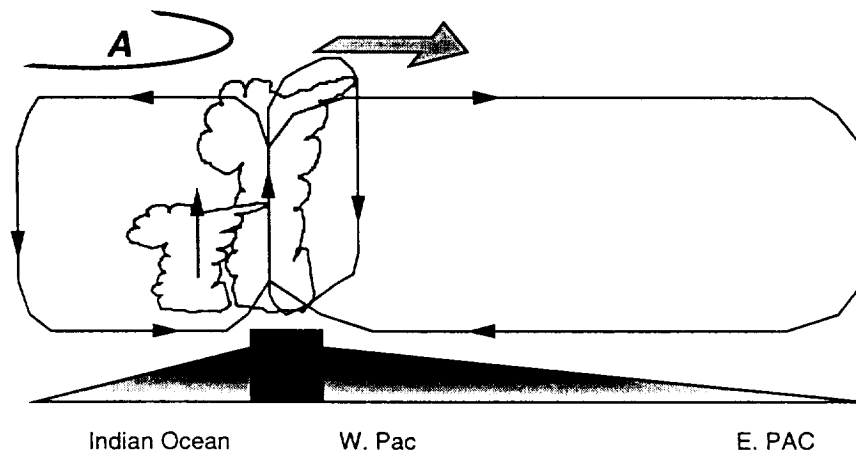   WY: Basin scale global monsoon/ENSO
        system

Indian Ocean   W. Pac   E. PAC

Fig. 23